Advances in Condensed Matter Physics

Exotic Superconductivity in Correlated Electron Systems

Guest Editors: Gang Mu, Viorel Sandu, Wei Li, and Bing Shen

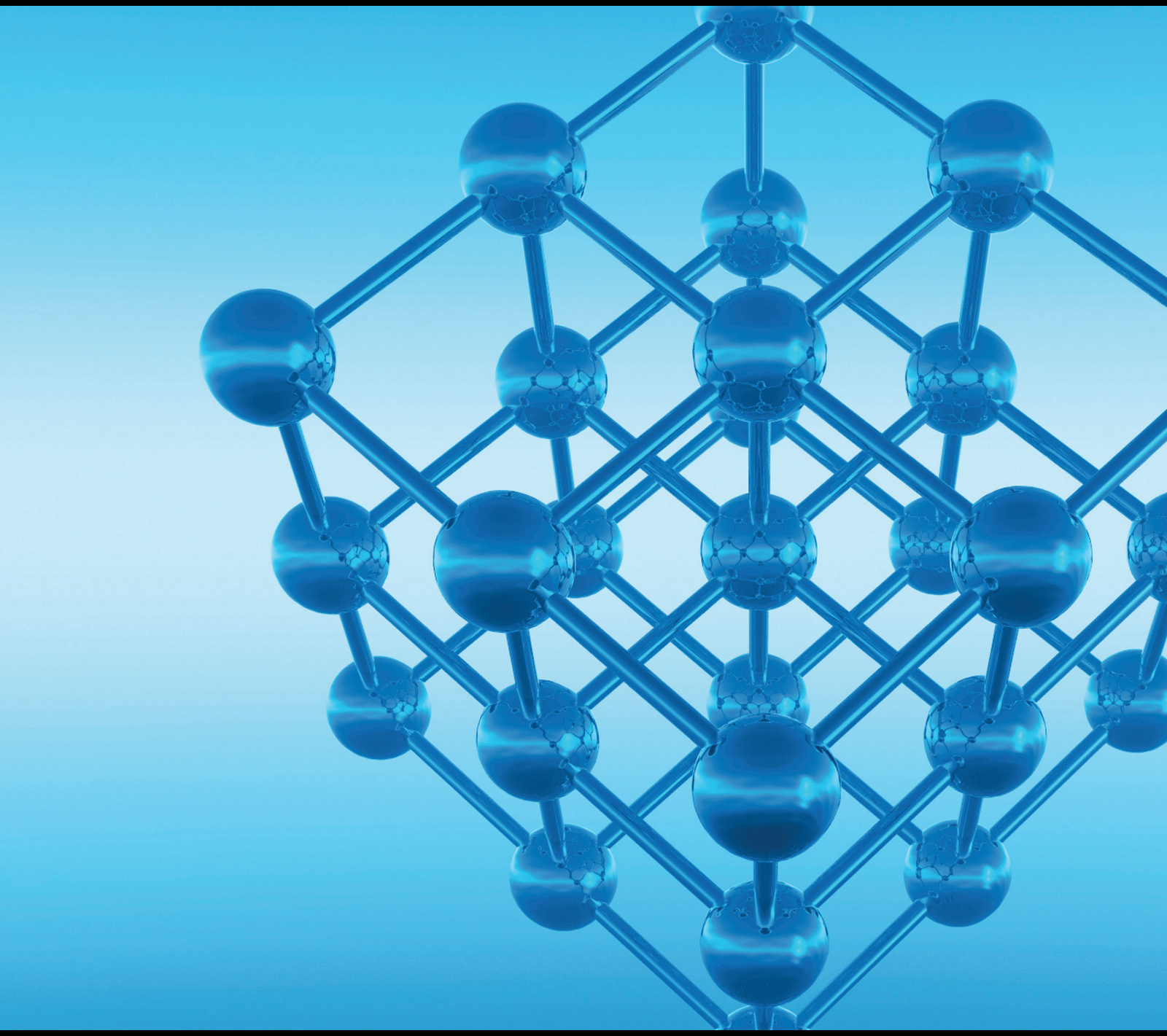

Exotic Superconductivity in Correlated Electron Systems

Advances in Condensed Matter Physics

Exotic Superconductivity in Correlated Electron Systems

Guest Editors: Gang Mu, Viorel Sandu, Wei Li, and Bing Shen

Editorial Board

Contents

Hindawi Publishing Corporation
Advances in Condensed Matter Physics
Volume 2015, Article ID 180195, 2 pages
http://dx.doi.org/10.1155/2015/180195

Editorial

Exotic Superconductivity in Correlated Electron Systems

Gang Mu,[1] Viorel Sandu,[2] Wei Li,[1] and Bing Shen[3]

[1]*State Key Laboratory of Functional Materials for Informatics and Shanghai Center for Superconductivity, Shanghai Institute of Microsystem and Information Technology, Chinese Academy of Sciences, Shanghai 200050, China*
[2]*National Institute of Materials Physics, 077125 Măgurele, Romania*
[3]*Argonne National Laboratory, Argonne, IL 60439, USA*

Correspondence should be addressed to Gang Mu; mugang@mail.sim.ac.cn

Received 25 May 2015; Accepted 25 May 2015

Over the past decades, the search for high-T_c superconductivity (SC) and its novel superconducting mechanisms is one of the most challenging tasks of condensed matter physicists and material scientists, wherein the most striking achievement is the discovery of high-T_c and unconventional superconductivity in strongly correlated 3d-electron systems, such as cuprates and iron pnictides/chalcogenides. Those exotic superconductors display the behaviors beyond the scope of the BCS theory (in the SC states) and the Landau-Fermi liquid theory (in the normal states). In general, such exotic superconductivity can be seen as correlated electron systems, where there are strong interplays among charge, spin, orbital, and lattice degrees of freedom. Thus, we focus on the exotic superconductivity in materials with correlated electrons in the present special issue.

To address the fruitful aspects in this special issue, we invited the authors ranging from experimentalists to theorists to submit their original researching papers. The topics also range from material synthetizing to physical investigations. In the former topic, two papers made efforts to explore new superconducting materials in different systems through different approaches. In the latter topic, one paper investigated the crystal field excitations in an iron-pnictide superconductor using the inelastic neutron scattering. Another two papers focused on the gap structure of the unconventional cuprates and iron-pnictide superconductors.

The paper by B. Li et al. reported pressure induced suppression to the valence change transition in a 4d-electron compound EuPdAs. Two-phase transitions at about 10 K and 180 K, respectively, were observed from resistivity and magnetic susceptibility measurements. They attempted to explore superconductivity in this system by applying pressure. They found that the transition at 180 K can be suppressed with a pressure as low as 0.48 GPa and no superconductivity has been induced with the pressure up to 1.90 GPa. Y. B. Sun et al. reported the insulator to superconductor transition in Ga-doped semiconductor Ge single crystal. The rapid thermal annealing was found to make Ga redistribute in the Ge matrix and realize the superconducting circuits. With increasing the annealing temperature, the samples show a crossover from the insulator to the superconductor. They argued that the Ga doped layer plays a leading role in the superconductivity.

Iron-pnictide superconductor $NdFeAsO_{0.85}F_{0.15}$ was investigated by P. Cheng et al. using inelastic neutron scattering measurements. They used the polycrystalline samples and the experiments were carried out over a wide temperature range of 3 K–250 K. They identified up to seven ground state crystal field excitations from the inelastic neutron spectra. A crystal field energy level scheme for Nd^{3+} was proposed. It shows quite different features comparing with that in tetragonal parent phase NdFeAsO. Their results indicate that the fluorine doping induced the superposition of crystal fields and lowered local point symmetries around the Nd^{3+}.

The symmetry and structure of the energy gap are one of the most important issues in the studies of the high-T_c and unconventional superconductors. Recently it was revealed by angle-resolved photoemission spectroscopy that the whole Fermi surface is fully gapped for several families of underdoped cuprates, which challenges the present theories

for the high-T_c superconductors. Based on a phenomenological model, T. Zhou et al. propose that the incommensurate diagonal spin-density-wave order can cause a finite gap along the d-wave nodal line. Their work gives a good explanation to the experimental observation. G. Mu et al. studied the gap structure of the iron-pnictide superconductor $Ba(Fe_{0.942}Ni_{0.058})_2As_2$ by the low-temperature specific heat measurements. A simple and reliable analysis shows that a clear T^2 term emerges in the low-temperature specific heat data. Their observation is similar to that observed in the Co-doped system in their previous work and is consistent with the theoretical prediction for a superconductor with line nodes in the energy gap.

Acknowledgments

At last, we sincerely acknowledge all the contributors for their hard work and patience in bringing out this special issue. We hope that the publication of this special issue will be of reference value for readers.

Gang Mu
Viorel Sandu
Wei Li
Bing Shen

Hindawi Publishing Corporation
Advances in Condensed Matter Physics
Volume 2015, Article ID 419017, 5 pages
http://dx.doi.org/10.1155/2015/419017

Research Article

Gap Structure of the Overdoped Iron-Pnictide Superconductor $Ba(Fe_{0.942}Ni_{0.058})_2As_2$: A Low-Temperature Specific-Heat Study

Gang Mu,[1] Bo Gao,[1] Xiaoming Xie,[1] Yoichi Tanabe,[2] Jingtao Xu,[3] Jiazhen Wu,[2] and Katsumi Tanigaki[2,3]

[1] *State Key Laboratory of Functional Materials for Informatics and Shanghai Center for Superconductivity, Shanghai Institute of Microsystem and Information Technology, Chinese Academy of Sciences, Shanghai 200050, China*
[2] *Department of Physics, Graduate School of Science, Tohoku University, Sendai 980-8578, Japan*
[3] *World Premier International Research Center, Tohoku University, Sendai 980-8578, Japan*

Correspondence should be addressed to Gang Mu; mugang@mail.sim.ac.cn and Katsumi Tanigaki; tanigaki@sspns.phys.tohoku.ac.jp

Received 15 December 2014; Accepted 11 March 2015

Academic Editor: Jörg Fink

Low-temperature specific heat (SH) is measured on the postannealed $Ba(Fe_{1-x}Ni_x)_2As_2$ single crystal with $x = 0.058$ under different magnetic fields. The sample locates on the overdoped sides and the critical transition temperature T_c is determined to be 14.8 K by both the magnetization and SH measurements. A simple and reliable analysis shows that, besides the phonon and normal electronic contributions, a clear T^2 term emerges in the low temperature SH data. Our observation is similar to that observed in the Co-doped system in our previous work and is consistent with the theoretical prediction for a superconductor with line nodes in the energy gap.

1. Introduction

The superconducting (SC) state of a superconductor is protected by an energy gap. The symmetry and structure of the energy gap can be very different in different SC materials. For the conventional superconductors (e.g., metallic superconductors), the gap is isotropic in the k space which is called the s-wave symmetry [1]. In some materials (e.g., MgB_2), multiple gaps have been discovered on different Fermi surfaces [2]. Highly anisotropic (the so-called d-wave) gap symmetry was confirmed in high-T_c cuprate superconductors [3]. The situation is more complicated in the iron-pnictide superconductors, because there are typically four or five bands crossing the Fermi level. Theoretically several candidates symmetries of the SC gaps were proposed [4], among which the so-called $S^{\pm}$ case seems to be accepted widely [5, 6]. On the experimental sides, the nodeless superconductivity has been confirmed in $(K, Tl)_xFe_{2-y}Se_2$ [7]. However, nodes (zero points) have been reported in the gaps of LaFePO, KFe_2As_2, and $BaFe_2(As_{1-x}P_x)_2$ [8–10]. At the same time, the consensus has not been reached on other systems of iron-pnictide superconductors [11–20]. In the electron doped (Co- or Ni-doped) 122 system, one tendency that the gap anisotropy becomes large and even gap nodes emerge in the overdoped samples has been reported by different groups and experimental methods [21–26].

Specific heat is a bulk tool to detect the quasiparticle density of states (DOS) at the Fermi level, which can provide information about the gap structure. The variation of the electronic SH in the SC states (C_{sc}) versus temperature can be rather different for different gap structures [27, 28]:

$$C_{sc} \sim \begin{cases} e^{-\Delta_0/k_BT}, & \text{s-wave} \\ T^2, & \text{line nodes} \\ T^3, & \text{point nodes,} \end{cases} \quad (1)$$

where Δ_0 is the magnitude of the energy gap. In order to segregate the pure electron SH from the measured mixed contributions, many methods have been tried [18, 29, 30]. In

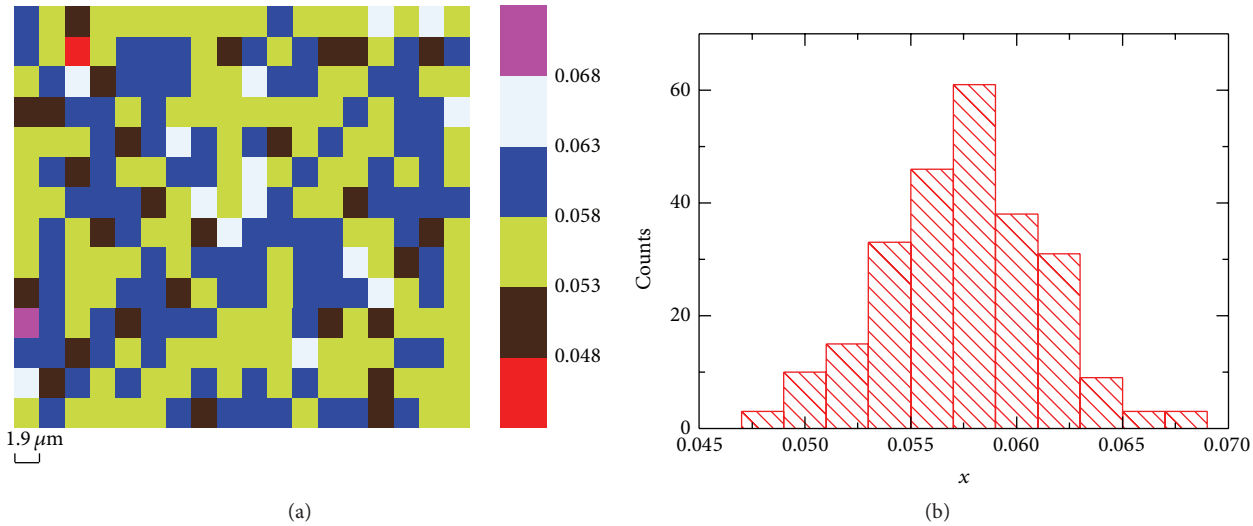

(a) (b)

FIGURE 1: (a) The mapping image (color online) of Ni concentration throughout an area of 38 μm × 28 μm based on the EDS quantitative results. (b) The chart of the Ni distributions summarized from same data as (a).

our previous work, we reported the clear presence of T^2 term in C_{el} of the overdoped $Ba(Fe_{1-x}\ Co_x)_2As_2$ from the raw data, giving a more solid evidence for the line-nodal gap structure [25, 26]. It is very important and necessary to investigate more systems with other dopants to check the universality of such a behavior.

In this paper, we studied the the low temperature SH of the Ni-doped $BaFe_2As_2$ in the overdoped region. Here we also observed a clear T^2 term in C_{sc}, being consistent with the theoretical prediction for the line-nodal superconductors. Our result along with the previous work indicates that it is a universal feature of the electron-doped 122 system.

2. Materials and Methods

The $Ba(Fe_{0.942}Ni_{0.058})_2As_2$ single crystal was grown by the self-flux method [31]. The as-grown sample was annealed under high vacuum at 1073 K for 20 days, because it was reported that the annealing process can improve the sample quality significantly [23]. The sample for the SH measurement has a mass of 2.9 mg. The actual Ni concentrations were checked and determined by the energy dispersive X-ray spectroscopy (EDS) measurements on a Bruker Quantax 200 system. The dc magnetization measurements were done with a superconducting quantum interference device (Quantum Design, MPMS7). The specific heat was measured with a Helium-3 system based on the physical property measurement system (Quantum Design, PPMS). We employed the thermal relaxation technique to perform the specific heat measurements. The thermometers have been calibrated under different magnetic fields beforehand. The external field was applied perpendicular to the c axis of the single crystal.

The distribution of the Ni-dopant on a microscale was investigated by EDS measurements. The mapping image of Ni concentration and the chart of its distributions throughout an area of 38 μm × 28 μm for our sample are shown in Figures 1(a) and 1(b). The spatial resolution is 1.9 μm. The distribution shows a peak at about 0.058, which is very close to the average value. Consequently, this value is taken as the actual doping level. The SC transition of the obtained single crystal was checked by the dc magnetization and specific heat measurements. As shown in Figure 2(a), the clear SC transition at about 14.8 K can be seen from both the M-T and C/T-T curves, indicating a high quality of the selected sample. Figure 2(b) shows schematically the phase diagram of the present Ni-doped system, which were reported by Ni et al. [32]. It is clear that our sample locates on the overdoped sides of the phase diagram and no magnetic order exists in this region, which supplies a clean platform to study the behaviors of specific heat.

3. Results and Discussion

We focus our attention on the SH data in the low temperature range to study the low-energy excitations. Generally speaking, in a system without magnetic order or magnetic impurities, the total SH is a simple integration of different components:

$$C(T) = \beta T^3 + C_{sc} + \gamma T. \quad (2)$$

The first term is the phonon SH, which is a very good approximation for the Debye model in the low temperature region. As mentioned in the introduction, the second term C_{sc} is the electronic SH in the SC states excited by the thermal energy. This is the most important and concerned in our study, because its responding behavior to temperature supplies the information of the gap structure. The third term is quite complicated. Under zero field, it is a residual electronic term typically coming from small amounts of nonsuperconducting content in the sample or impurity scattering in some unconventional superconductors [3, 33]. With a field higher than the lower critical field, it reflects the contribution of the

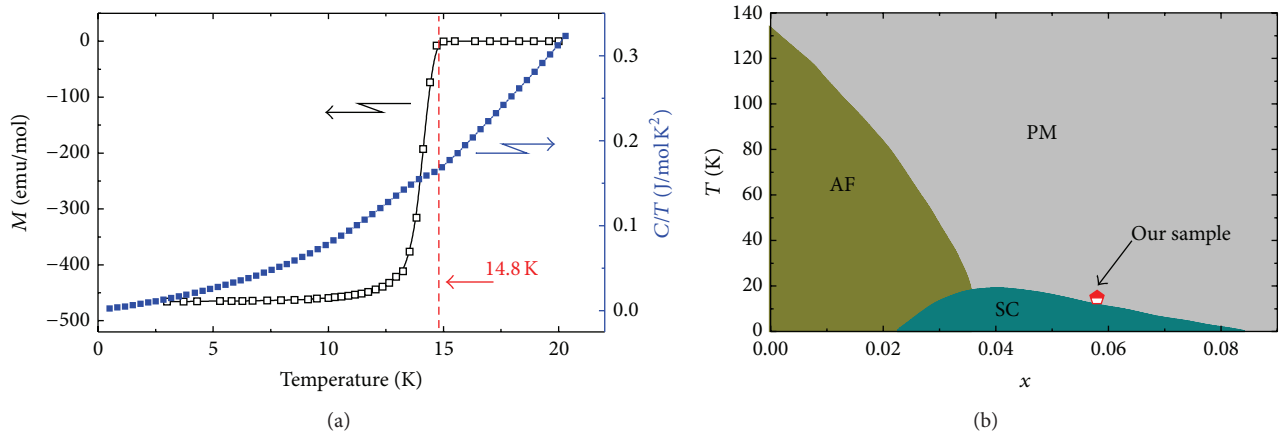

FIGURE 2: (a) Temperature dependence (color online) of dc magnetization (left) and specific heat coefficient C/T (right) for the sample. The magnetization data are collected with field $H = 10$ Oe using the zero field cooling (ZFC) process. (b) Phase diagram for the Ni-doped 122 system [32]. The red mark shows the location of our sample.

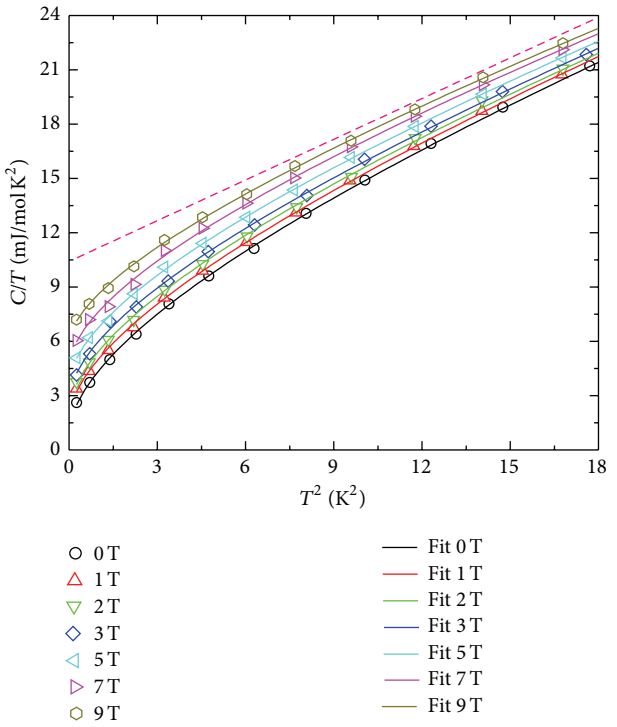

FIGURE 3: The raw data (color online) of the SH under different fields in the low temperature region. The data are shown in C/T versus T^2 plot. The solid lines display the theoretical fitting (see text). The dashed straight line is the guide for the eyes.

vortex states. Here we plot the raw data of SH as C/T versus T^2 in Figure 3. A clear feature in this figure is the negative curvature in all the curves under different fields, rather than a linear behavior as revealed by the dashed pink line. This behavior is not expected for the SC gap with s-wave symmetry or point nodes. In the case of s-wave, the value of C_{sc} is negligibly small in the low temperature region due to the exponential relation. For systems with point nodes, the contribution of C_{sc} has the same T^3-dependence as the phonon term. In both cases, the C/T-T^2 curves should show a linear behavior in the present low temperature region. Intuitively, the case of gap with line nodes is the best candidate. Consequently, we fitted our data using (2) based on the line-nodal situation ($C_{sc} = \alpha T^2$). As represented by the solid lines, the fitting results are shown in Figure 3. One can see that the fitting curves coincide the experimental data very well. This gives a direct evidence for the presence of line nodes in the energy gap.

To further confirm the reliability of the analysis, we checked the obtained fitting parameters carefully. We show the field dependence of the parameters β, α, and γ in Figures 4(a), 4(b), and 4(c), respectively. The value of β is almost independent of field, which is reasonable because magnetic field cannot affect the phonon SH. Moreover, $\alpha(H)$ decreases monotonously with the increase of magnetic field up to 9 T. This is similar to that observed in overdoped $Ba(Fe_{1-x}\ Co_x)_2As_2$ and has been attributed to the combined effects imposed by the three-dimension dispersion of the line nodes on the Fermi surface and the destruction of V-shape of the density of states (DOS) at the nodes by the field [25, 26]. The residual value of γ under zero field (denoted as γ_0) is estimated to be 0.75 mJ/mol K^2, which is also comparable to the reports in overdoped $Ba(Fe_{1-x}\ Co_x)_2As_2$ and suggests a high sample quality. A clear increase of γ with the field is observed. It is difficult to describe the field dependence of γ using a simple formula due to the multiband effect in the present system. Qualitatively, γ increases more quickly in the system with a highly anisotropic gap. At the present stage, we could not evaluate the information supplied by the field dependent data, since the upper critical field H_{c2} and the normal state electronic SH coefficient γ_n are not clear.

The clear data and reasonable fitting parameters give us the confidence about the credibility of the present analysis process. More importantly, very few fitting parameters are involved in this approach. However, we cannot obtain the precise location of the line nodes, since SH measurements integrate the information from different directions of the

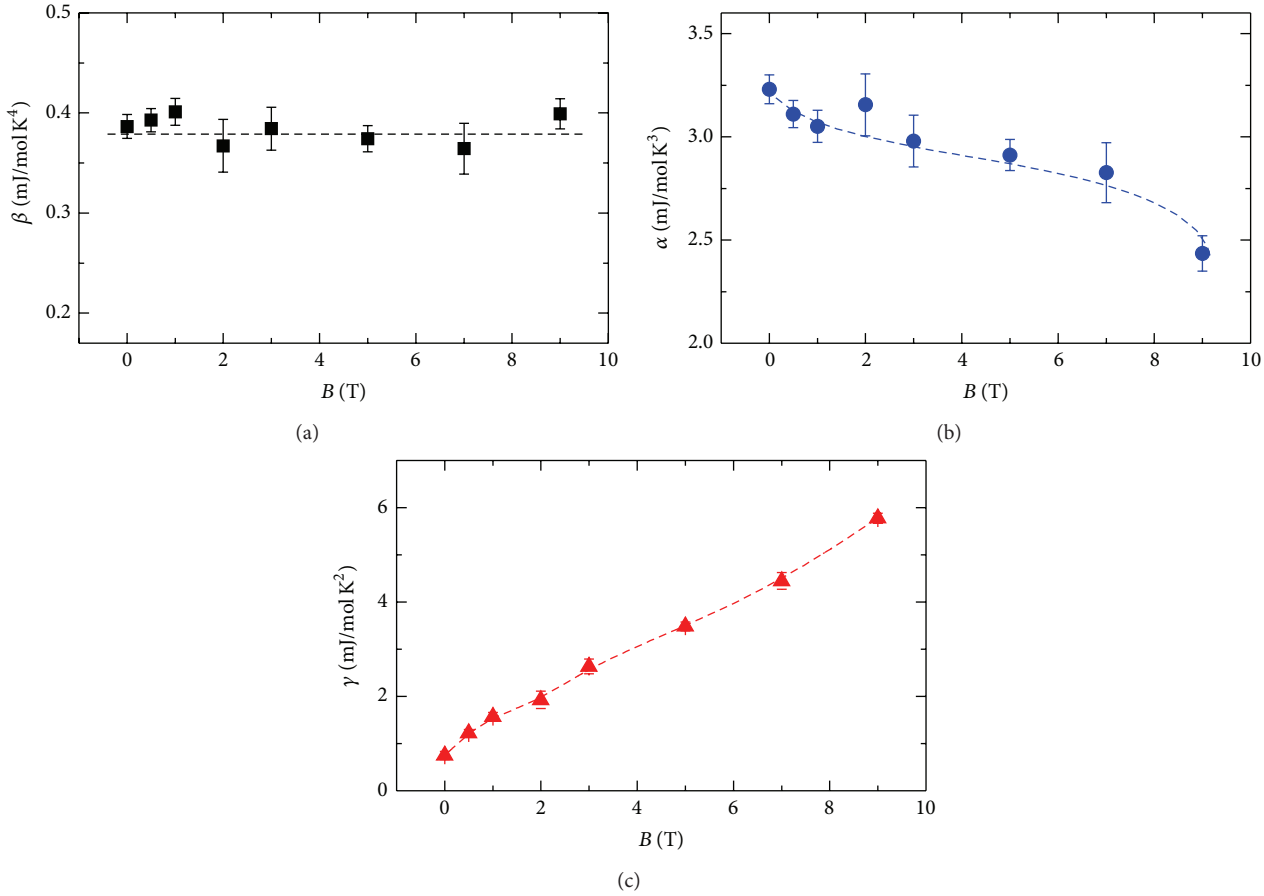

FIGURE 4: Field dependence (color online) of the fitting parameters β and α and γ.

Fermi surface. Most likely, the magnitude and structure of the gaps on different Fermi surfaces are rather different. We must emphasize that such a multiband does not destroy the validity of our analysis results because the electronic SH from the Fermi pockets with line nodes will prevail against that from fully gapped pockets in the low temperature limit.

In summary, we studied the low-temperature specific heat on the $Ba(Fe_{1-x}\ Ni_x)_2As_2$ single crystal with $x = 0.058$. Before measurements, the single crystals were carefully annealed to improve the sample quality. We found a clear evidence for the presence of T^2 term from the raw SH data, which is consistent with the theoretical prediction for the superconductors with line nodes. Our result is very similar to the previous reports on the Co-doped system. Future investigations on other systems of the iron-pnictide superconductors are needed to check whether it is a common feature for the presence of line nodes on the overdoped sides of the electron-doped 122 system.

Conflict of Interests

The authors declare that there is no conflict of interests regarding the publication of this paper.

Acknowledgments

This work is supported by the Natural Science Foundation of China (Grant no. 11204338) and the "Strategic Priority Research Program (B)" of the Chinese Academy of Sciences (Grants nos. XDB04040300 and XDB04030000). Gang Mu expresses special thanks to Grants-in-Aid for Scientific Research from the Japan Society for the Promotion of Science (JSPS) (Grant no. P10026).

References

[1] G. Mu, Y. Wang, L. Shan, and H.-H. Wen, "Possible nodeless superconductivity in the noncentrosymmetric superconductor $Mg_{12-\delta}\ Ir_{19}\ B_{16}$," *Physical Review B*, vol. 76, no. 6, Article ID 064527, 2007.

[2] F. Bouquet, R. A. Fisher, N. E. Phillips, D. G. Hinks, and J. D. Jorgensen, "Specific heat of $Mg^{11}B_2$: evidence for a second energy gap," *Physical Review Letters*, vol. 87, no. 4, Article ID 047001, 2001.

[3] H.-H. Wen, Z.-Y. Liu, F. Zhou et al., "Electronic specific heat and low-energy quasiparticle excitations in the superconducting state of $La_{2-x}Sr_xCuO_4$ single crystals," *Physical Review B*, vol. 70, no. 21, Article ID 214505, 2004.

[4] P. J. Hirschfeld, M. M. Korshunov, and I. I. Mazin, "Gap symmetry and structure of Fe-based superconductors," *Reports on Progress in Physics*, vol. 74, no. 12, Article ID 124508, 2011.

[5] I. I. Mazin, D. J. Singh, M. D. Johannes, and M. H. Du, "Unconventional superconductivity with a sign reversal in the order parameter of $LaFeAsO_{1-x}F_x$," *Physical Review Letters*, vol. 101, no. 5, Article ID 057003, 2008.

[6] K. Kuroki, S. Onari, R. Arita et al., "Erratum: unconventional pairing originating from the disconnected fermi surfaces of superconducting $LaFeAsO_{1-x}F_x$," *Physical Review Letters*, vol. 102, no. 10, Article ID 109902, 2009.

[7] D. Mou, S. Liu, X. Jia et al., "Distinct Fermi surface topology and nodeless superconducting gap in a (Tl0.58Rb0.42)Fe1.72Se2 superconductor," *Physical Review Letters*, vol. 106, no. 10, Article ID 107001, 2011.

[8] J. D. Fletcher, A. Serafin, L. Malone et al., "Evidence for a nodal-line superconducting state in LaFePO," *Physical Review Letters*, vol. 102, no. 14, Article ID 147001, 2009.

[9] J. K. Dong, S. Y. Zhou, T. Y. Guan et al., "Quantum criticality and nodal superconductivity in the FeAs-based superconductor KFe_2As_2," *Physical Review Letters*, vol. 104, no. 8, Article ID 087005, 2010.

[10] Y. Zhang, Z. R. Ye, Q. Q. Ge et al., "Nodal superconducting-gap structure in ferropnictide superconductor $BaFe_2(As0.7P0.3)_2$," *Nature Physics*, vol. 8, no. 5, pp. 371–375, 2012.

[11] Y.-L. Wang, L. Shan, L. Fang, P. Cheng, C. Ren, and H.-H. Wen, "Multiple gaps in $SmFeAsO_{0.9}F_{0.1}$ revealed by point-contact spectroscopy," *Superconductor Science and Technology*, vol. 22, no. 1, Article ID 015018, 2009.

[12] T. Sato, S. Souma, K. Nakayama et al., "Superconducting gap and pseudogap in iron-based layered superconductor $La(O_{1-x}F_x)FeAs$," *Journal of the Physical Society of Japan*, vol. 77, no. 6, Article ID 063708, 2008.

[13] S. Kawasaki, K. Shimada, G. F. Chen, J. L. Luo, N. L. Wang, and G.-Q. Zheng, "Two superconducting gaps in $LaFeAsO_{0.92}F_{0.08}$ revealed by ^{75}As nuclear quadrupole resonance," *Physical Review B*, vol. 78, no. 22, Article ID 220506, 2008.

[14] G. Mu, X. Zhu, L. Fang et al., "Nodal gap in Fe-based layered superconductor $LaO_{0:9}F_{0.1-\delta}FeAs$ probed by specific heat measurements," *Chinese Physics Letters*, vol. 25, pp. 2221–2224, 2008.

[15] T. Y. Chen, Z. Tesanovic, R. H. Liu, X. H. Chen, and C. L. Chien, "A BCS-like gap in the superconductor $SmFeAsO_{0.85}F_{0.15}$," *Nature*, vol. 453, no. 7199, pp. 1224–1227, 2008.

[16] H. Ding, P. Richard, K. Nakayama et al., "Observation of Fermi-surface-dependent nodeless superconducting gaps in $Ba_{0.6}K_{0.4}Fe_2As_2$," *Europhysics Letters*, vol. 83, no. 4, Article ID 47001, 2008.

[17] K. Hashimoto, T. Shibauchi, T. Kato et al., "Microwave penetration depth and quasiparticle conductivity of $PrFeAsO_{1-y}$ single crystals: evidence for a full-gap superconductor," *Physical Review Letters*, vol. 102, no. 1, Article ID 017002, 2009.

[18] G. Mu, H. Luo, Z. Wang, L. Shan, C. Ren, and H.-H. Wen, "Low temperature specific heat of the hole-doped $Ba_{0.6}K_{0.4}Fe_2As_2$ single crystals," *Physical Review B: Condensed Matter and Materials Physics*, vol. 79, no. 17, Article ID 174501, 2009.

[19] J.-P. Reid, M. A. Tanatar, X. G. Luo et al., "Nodes in the gap structure of the iron arsenide superconductor $Ba(\mathbf{Fe_{1-x}Co_x})_2As_2$ from c -axis heat transport measurements," *Physical Review B—Condensed Matter and Materials Physics*, vol. 82, Article ID 064501, 2010.

[20] B. Zeng, G. Mu, H. Q. Luo et al., "Anisotropic structure of the order parameter in $FeSe_{0.45}Te_{0.55}$ revealed by angle-resolved specific heat," *Nature Communications*, vol. 1, no. 8, article 112, 2010.

[21] C. Martin, H. Kim, R. T. Gordon et al., "Evidence from anisotropic penetration depth for a three-dimensional nodal superconducting gap in single-crystalline $Ba(Fe_{1---x}Ni_x)_2As_2$," *Physical Review B—Condensed Matter and Materials Physics*, vol. 81, no. 6, Article ID 060505, 2010.

[22] J.-P. Reid, M. A. Tanatar, X. G. Luo et al., "Nodes in the gap structure of the iron arsenide superconductor $Ba(Fe_{1-x}Co_x)2As2$ from c-axis heat transport measurements," *Physical Review B: Condensed Matter and Materials Physics*, vol. 82, no. 6, Article ID 064501, 2010.

[23] K. Gofryk, A. B. Vorontsov, I. Vekhter et al., "Effect of annealing on the specific heat of $Ba(Fe_{1-x}Co_x)_2As_2$," *Physical Review B*, vol. 83, no. 6, Article ID 064513, 2011.

[24] T. Fischer, A. V. Pronin, J. Wosnitza et al., "Highly anisotropic energy gap in superconducting $Ba(Fe_{0.9}Co_{0.1})_2As_2$ from optical conductivity measurements," *Physical Review B*, vol. 82, no. 22, Article ID 224507, 2010.

[25] G. Mu, J. Tang, Y. Tanabe, J. Xu, S. Heguri, and K. Tanigaki, "Evidence for line nodes in the energy gap of the overdoped $Ba(Fe_{1-x}Co_x)_2As_2$ from low-temperature specific heat measurements," *Physical Review B: Condensed Matter and Materials Physics*, vol. 84, no. 5, Article ID 054505, 2011.

[26] G. Mu, J. Tang, Y. Tanabe et al., "A field-directional specific heat study on the gap structure of overdoped $Ba(Fe_{1-x}Co_x)_2As_2$," *Journal of the Physical Society of Japan*, vol. 82, no. 5, Article ID 054714, 2013.

[27] M. Sigrist and K. Ueda, "Phenomenological theory of unconventional superconductivity," *Reviews of Modern Physics*, vol. 63, no. 2, pp. 239–311, 1991.

[28] N. E. Hussey, "Low-energy quasiparticles in high-T_c cuprates," *Advances in Physics*, vol. 51, no. 8, pp. 1685–1771, 2002.

[29] P. Popovich, A. V. Boris, O. V. Dolgov et al., "Specific heat measurements of $Ba_{0.68}K_{0.32}Fe_2As_2$ single crystals: evidence for a multiband strong-coupling superconducting state," *Physical Review Letters*, vol. 105, no. 2, Article ID 027003, 2010.

[30] K. Gofryk, A. S. Sefat, M. A. McGuire et al., "Doping-dependent specific heat study of the superconducting gap in $Ba(Fe_{1-x}Co_x)_2As_2$," *Physical Review B*, vol. 81, no. 18, Article ID 184518, 2010.

[31] L. Fang, H. Luo, P. Cheng et al., "Roles of multiband effects and electron-hole asymmetry in the superconductivity and normal-state properties of $Ba(Fe_{1-x}Co_x)_2As_2$," *Physical Review B*, vol. 80, no. 14, Article ID 140508, 2009.

[32] N. Ni, A. Thaler, J. Q. Yan et al., "Temperature versus doping phase diagrams for $Ba(Fe_{1-x}TM_x)_2As_2$(TM = Ni,Cu,Cu/Co) single crystals," *Physical Review B*, vol. 82, Article ID 024519, 2010.

[33] G. Mu, B. Zeng, P. Cheng et al., "Sizable residual quasiparticle density of states induced by impurity scattering effect in $Ba(Fe_{1-x}Co_x)_2As_2$ single crystals," *Chinese Physics Letters*, vol. 27, no. 3, Article ID 037402, 2010.

Hindawi Publishing Corporation
Advances in Condensed Matter Physics
Volume 2015, Article ID 575421, 4 pages
http://dx.doi.org/10.1155/2015/575421

Research Article

Pressure Induced Suppression to the Valence Change Transition in EuPdAs

Baoxuan Li, Jianzhong Liu, Yufeng Li, Xiyu Zhu, and Hai-Hu Wen

Center for Superconducting Physics and Materials, National Laboratory of Solid State Microstructures and Department of Physics, National Center of Microstructures and Quantum Manipulation, Nanjing University, Nanjing 210093, China

Correspondence should be addressed to Hai-Hu Wen; hhwen@nju.edu.cn

Received 6 December 2014; Accepted 8 February 2015

Academic Editor: Viorel Sandu

By applying a hydrostatic pressure, we have successfully suppressed the valence change transition in EuPdAs. The studied compound EuPdAs crystallizes in a P63/mmc space group. Through resistivity and magnetic susceptibility measurements, we find that EuPdAs shows a phase transition at 180 K and another transition below 10 K at ambient pressure, as was reported before. The overall transport and magnetic behavior is to some extent similar to that of the parent phase of iron based superconductors. With application of a hydrostatic pressure, the transition at 180 K is sensitively suppressed with a pressure as low as 0.48 GPa. However, superconductivity has not been induced with pressure up to 1.90 GPa.

1. Introduction

The EuPdAs alloy adopts the hexagonal $CaIn_2$-type structure. The transport and magnetic measurements of this material reveal a similarity to the parent phase of iron based superconductors [1, 2]. Particularly, there is a clear transition at around 180 K, which is of first order and accompanied with a large volume collapse caused by a strong contraction of the c-axis [3–5]. The transition at 180 K was reported to be induced by the fluctuation of Eu valence from 2.15 to 2.40 between 300 K and 4 K as revealed by experiments of Moessbauer measurement and μSR method [3, 6, 7]. However, whether this transition is related to some kind of magnetic transition is still unclear. And as it is known in the iron based superconductors, there is a close relationship between the high temperature phase transition and the emergence of superconductivity [8, 9]. Inspired by this similarity, we intend to check whether the transition at 180 K can be suppressed under hydrostatic pressure, as many iron-based superconductors do, and, if the transition is really related to a certain magnetic transition, whether superconductivity can be induced with the suppression of the transition.

2. Experimental Details

The polycrystalline sample of EuPdAs was synthesized by solid state reaction method, using EuAs as the precursor made by reaction of Eu and As (purity 99.9%, Alfa Aesar). High purity EuAs and Pd powder (99.99% purity, Cuibolin) were weighed in stoichiometric ratio, mixed well, and pressed into a pellet in an argon filled glove box. The pellet was loaded into an alumina crucible, which was sealed in an evacuated quartz ampule and then kept inside a PID controlled furnace. The temperature of the furnace was raised to 1000°C with a heating rate of 1.2°C/min and maintained for 24 hours. The sintered sample was cooled down naturally to room temperature with the furnace power turned off from 1000°C.

X-ray diffraction (XRD) measurements were performed on a Bruker D8 advanced diffractometer with the Cu-K_α radiation. Dc magnetization measurements were carried out with a SQUID-VSM-7T (Quantum Design). Measurements of resistivity under pressure were performed up to 2.3 GPa on a physical property measurement system (PPMS-16T, Quantum Design) by using HPC-33 piston type pressure cell with the Quantum Design dc resistivity and ac transport options. For the resistive measurements, silver leads with a diameter of 50 μm were glued to the EuPdAs sample in a standard four-probe method by using silver epoxy, and the sample was immersed in the pressure transmitting medium (Daphne 7373) in a Teflon cap with a diameter of 4 mm. Hydrostatic pressure was generated by a BeCu/NiCrAl clamped piston-cylinder cell. The pressure upon the sample was calibrated

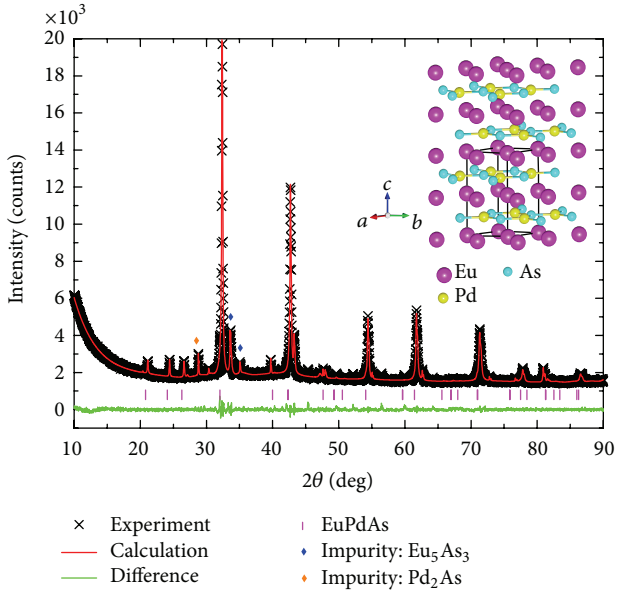

Figure 1: Powder X-ray diffraction patterns and the Rietveld refinement profile of the EuPdAs sample at room temperature. All main diffraction peaks can be indexed well by the P63/mmc space group (hexagonal structure) with $a = 4.262$ Å and $c = 8.535$ Å with Eu_5As_3 and Pd_2As as the impurity phases. The ratio between EuPdAs and the impurities is found to be 90 : 10.

with the shift in T_c of a high purity Sn sample by measuring the temperature dependence of resistivity.

3. Results and Discussion

Figure 1 shows the powder XRD patterns of the EuPdAs sample at room temperature, along with the result of the Rietveld structural refinement using the TOPAS program. On the whole, it is clear that the main diffraction peaks can be indexed well by a hexagonal cell structure with the P63/mmc space group. In addition to a principal phase, some weak peaks arising from the impurity phases of Eu_5As_3 and Pd_2As can also be seen. A detailed fitting to the structural data shows that the ratio between EuPdAs and the impurity phases is around 90 : 10 for this sample. The refined lattice parameters are extracted to be $a = 4.262$ Å and $c = 8.535$ Å.

Figure 2(a) shows the temperature dependence of zero-field-cooled (ZFC) and field-cooled (FC) dc magnetic susceptibility for EuPdAs under 20 Oe. An anomaly can be clearly seen around 8 K, where the ZFC curve shows some deviation from the FC curve; this may be an indication of long range magnetic ordering of Eu ions. We can also observe a kink at around 5.4 K, which has not been reported before. We conjecture that the 5.4 K kink may be a secondary transition of the Eu ions ordering, but we cannot rule out the possibility that this anomaly arises from the impurity phases of Eu_5As_3 or Pd_2As. Figure 2(b) shows the temperature dependence of ZFC magnetic susceptibility under 1T. In addition to the susceptibility saturation below 10 K, corresponding to the 8 K anomaly in Figure 2(a), there is another kink around 180 K, which can be easily observed in the inset of Figure 2(b). And above 180 K, the magnetic susceptibility of EuPdAs follows Curie-Weiss law behavior very well.

The temperature dependence of electrical resistivity for EuPdAs with temperature ranging from 2.3 K to 300 K is shown in Figure 3. The 8 K and 180 K kinks also clearly appear in these resistivity curves, which is consistent with the magnetic measurements (while the 5.4 K anomaly is absent in the resistive curve). The overall transport behavior, especially the 180 K anomaly, reminds us of some parent phases of iron-based materials, like $BaFe_2As_2$, which exhibits antiferromagnetic order originated from Fe ions around 140 K. When we apply pressure or do some chemical substitutions on $BaFe_2As_2$, the 140 K transition will be gradually suppressed to lower temperature, eventually, the antiferromagnetic transition will totally disappear and superconducting state will be induced [2, 10].

Inspired by the knowledge in the parent phase of iron based superconductors, we suspect that the 180 K anomaly for EuPdAs may be related to some kind of magnetic order of the Pd ions. If we can find some way to suppress this transition, we may expect some interesting properties, like superconductivity. To realize this purpose, we try to apply a hydrostatic pressure to EuPdAs.

The temperature dependence of resistivity for EuPdAs at various pressures with temperature ranging from 2.3 K to 250 K is illustrated in Figure 4. We find that the transition at 180 K is totally suppressed with a pressure of 0.48 GPa, and the resistivity value is depressed monotonously upon increasing pressure. However, no superconducting transition has been observed with pressure up to 1.90 GPa, while the 8 K anomaly is always preserved. Since the 180 K transition is so sensitive to pressure, we deem that it is merely a valence change transition and may not relate to the formation of any long range magnetic order. In addition, the 180 K anomaly can completely recover when pressure is removed (see Figure 3, the red curve); this reminds us of some pressure-induced iron-based superconductors, like $CaFe_2As_2$, in which the crystal structure will completely recover with pressure removed [11].

It is reported that the transition at 180 K is accompanied with a giant volume collapse of 1.9% caused by a strong contraction of the c-axis (2.3%) between 180 K and 150 K [3–5]; on the other hand, the lattice parameters will experience a strong but continuous decrease with increasing pressure [12]. Under the above considerations, it is reasonable to assume that the pressure we applied can result in the volume collapse at room temperature, which may induce the valence shift to 2.4 to occur at much higher temperature. Thus when applying pressure, the behaviour of the resistivity curve is well preserved below 180 K, while the 180 K transition disappears and the curve above 180 K extends smoothly from that at lower temperature.

The resistivity of the system is generally about 100–300 $\mu\Omega$cm, which manifests that the sample can be categorized as a bad metal. Since Eu has usually an ionic state of Eu^{2+} and/or Eu^{3+}, while the As can stay at several anionic states such as As^{3-} and As^{1-}, in this case the ionic state of Pd can be

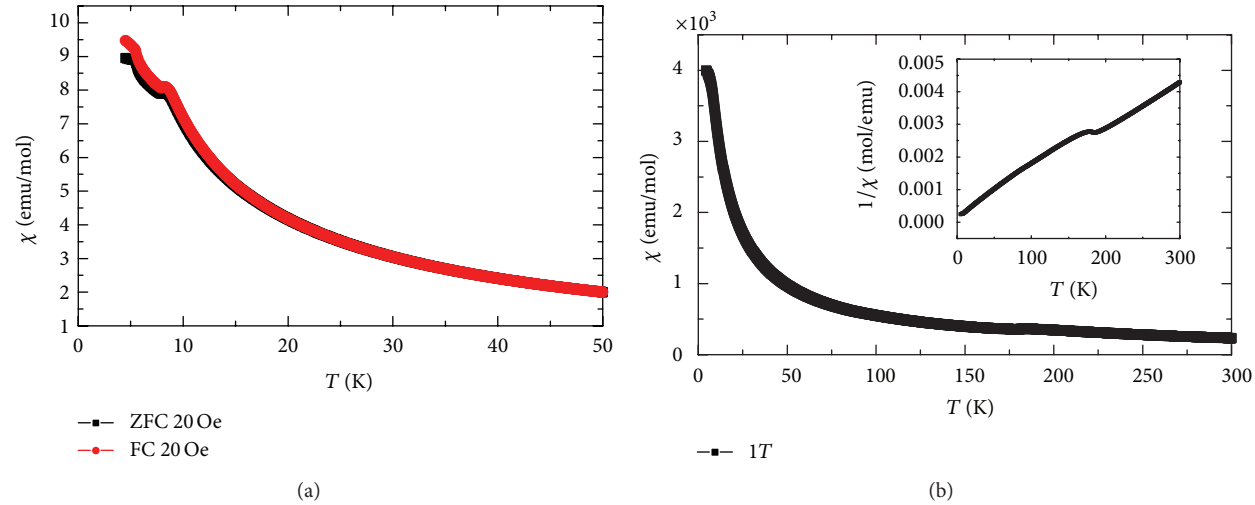

FIGURE 2: (a) Temperature dependence of dc magnetic susceptibility for EuPdAs as measured at an applied magnetic field of 20 Oe in the temperature range of 4.5 K to 50 K. Both magnetic susceptibilities measured in zero-field-cooled (ZFC) and field-cooled (FC) modes are shown. (b) Temperature dependence of dc magnetic susceptibility for EuPdAs under 1T in the temperature range of 4.5 K to 300 K. The inset shows $1/\chi$ versus T to clarify the 180 K anomaly.

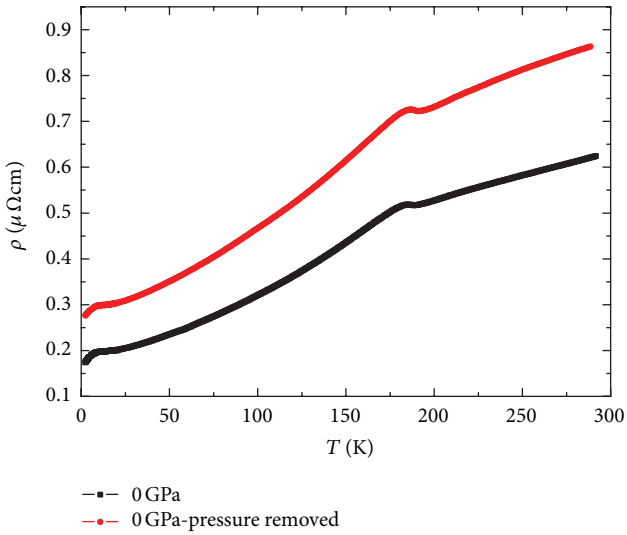

FIGURE 3: Temperature dependence of electrical resistivity for EuPdAs in the temperature range 2.3 K to 300 K (the black curve). The red curve is the result measured after pressure is removed (sample still immersed in the pressure transmitting medium).

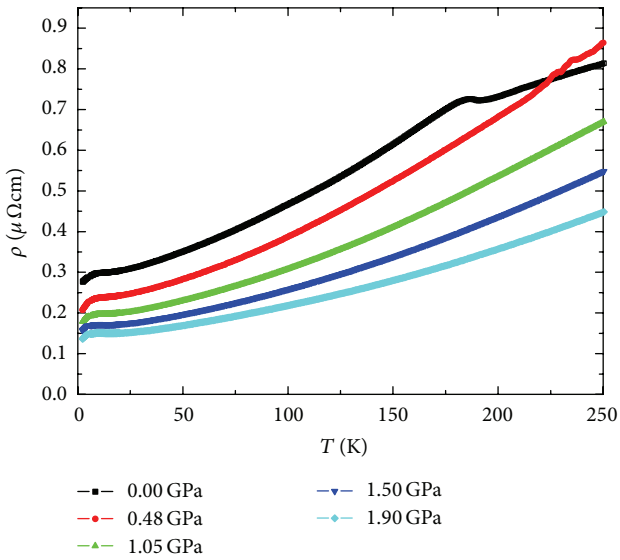

FIGURE 4: Temperature dependence of electrical resistivity for EuPdAs at various pressures in the temperature range 2.3 K to 250 K.

widely tuned. This provides a good way to tune the electronic states of the materials. This may provide an explanation to the transition at around 180 K, which is most probably induced by a valence change effect. From our recent study, one can see that the magnetic moment detected in the material is quite weak, either from the Pd or Eu ions. Nor has the long range magnetic order formation been found on the Pd ions. It would be interesting to use chemical doping to tune the electronic state 4d orbital in order to achieve a good balance between the itinerancy and local magnetism.

4. Conclusion

In summary, we have synthesized polycrystalline samples of EuPdAs by solid state reaction method. Through resistivity and magnetic susceptibility measurements, we find that EuPdAs shows a phase transition at 180 K, as well as a second phase transition below 10 K at ambient pressure. With application of hydrostatic pressure, the transition at 180 K is totally suppressed under a pressure of 0.48 GPa, and the resistivity curve is depressed monotonously upon increasing pressure. However, superconductivity has not been induced at low temperature with pressure up to 1.90 GPa. In order to achieve

some novel electronic properties, such as superconductivity, we suggest that tuning the occupation of the 4d orbitals of Pd with electrons would be essential.

Conflict of Interests

The authors declare that there is no conflict of interests regarding the publication of this paper.

References

[1] L. J. Li, Y. K. Luo, Q. B. Wang et al., "Superconductivity induced by Ni doping in $BaFe_2As_2$ single crystals," *New Journal of Physics*, vol. 11, Article ID 025008, 2009.

[2] P. C. Canfield and S. L. Bud'ko, "FeAs-based superconductivity: a case study of the effects of transition metal doping on $BaFe_2As_2$," *Annual Review of Condensed Matter Physics*, vol. 1, pp. 27–50, 2010.

[3] G. Michels, S. Junk, N. Lossau et al., "Mixed valency and first order phase transition in EuPdAs," *Zeitschrift für Physik B Condensed Matter*, vol. 86, pp. 53–58, 1992.

[4] D. Johrendt and A. Mewis, "Darstellung und kristallstrukturen der verbindungen SEPdAs (SELa-Lu)," *Journal of Alloys and Compounds*, vol. 183, pp. 210–223, 1992.

[5] G. Michels, C. Huhnt, W. Scharbrodt et al., "Temperature and pressure driven valence change in ternary Eu-pnictides," *Physica B: Physics of Condensed Matter*, vol. 206-207, pp. 408–411, 1995.

[6] H.-H. Klauß, M. Hillberg, W. Wagener et al., "Valence fluctuations in ternary europium compounds," *Hyperfine Interactions*, vol. 104, no. 1–4, pp. 171–175, 1997.

[7] V. Kataev, G. Khaliullin, G. Michels et al., "ESR study of the electronic properties of ternary europium pnictides," *Journal of Magnetism and Magnetic Materials*, vol. 137, no. 1-2, pp. 157–166, 1994.

[8] J. Paglione and R. L. Greene, "High-temperature superconductivity in iron-based materials," *Nature Physics*, vol. 6, no. 9, pp. 645–658, 2010.

[9] F. Wang and D.-H. Lee, "The electron-pairing mechanism of iron-based superconductors," *Science*, vol. 332, no. 6026, pp. 200–204, 2011.

[10] H. Fukazawa, N. Takeshita, T. Yamazaki et al., "Suppression of magnetic order by pressure in $BaFe_2As_2$," *Journal of the Physical Society of Japan*, vol. 77, no. 10, Article ID 105004, 2008.

[11] H. Lee, E. Park, T. Park et al., "Pressure-induced superconducting state of antiferromagnetic $CaFe_2$ As_2," *Physical Review B—Condensed Matter and Materials Physics*, vol. 80, no. 2, Article ID 024519, 2009.

[12] C. Huhnt, G. Michels, W. Schlabitz, D. Johrendt, and A. Mewis, "Pressure-driven valence change in ternary Eu pnictides," *Journal of Physics Condensed Matter*, vol. 9, no. 45, pp. 9953–9960, 1997.

Hindawi Publishing Corporation
Advances in Condensed Matter Physics
Volume 2015, Article ID 652424, 8 pages
http://dx.doi.org/10.1155/2015/652424

Research Article

"Nodal Gap" Induced by the Incommensurate Diagonal Spin Density Modulation in Underdoped High-T_c Superconductors

Tao Zhou,[1] Yi Gao,[2] and Jian-Xin Zhu[3]

[1]*College of Science, Nanjing University of Aeronautics and Astronautics, Nanjing 210016, China*
[2]*Department of Physics and Institute of Theoretical Physics, Nanjing Normal University, Nanjing 210023, China*
[3]*Theoretical Division and Center for Integrated Nanotechnologies, Los Alamos National Laboratory, Los Alamos, NM 87545, USA*

Correspondence should be addressed to Tao Zhou; tzhou@nuaa.edu.cn

Received 31 December 2014; Accepted 7 March 2015

Academic Editor: Viorel Sandu

Recently it was revealed that the whole Fermi surface is fully gapped for several families of underdoped cuprates. The existence of the finite energy gap along the d-wave nodal lines (nodal gap) contrasts the common understanding of the d-wave pairing symmetry, which challenges the present theories for the high-T_c superconductors. Here we propose that the incommensurate diagonal spin-density-wave order can account for the above experimental observation. The Fermi surface and the local density of states are also studied. Our results are in good agreement with many important experiments in high-T_c superconductors.

The energy gap is one of the most important properties in the studies of the high-T_c superconductors. Recently, measurements of the energy gaps by angle-resolved photoemission spectroscopy (ARPES) in lightly doped high-T_c materials revealed the existence of the nonzero energy gap along the diagonal directions of the Brillouin zone (also referred to as the "nodal gap") [1–6]. The earliest indication of fully gapped single-particle excitation was reported in [7]. The existence of the nodal gap seems to be generic. It has been observed in several families of cuprates [1–7]. Moreover, it has been reported that the nodal gap exists in the antiferromagnetic (AF) state [5, 6], the spin glass region [3], and the superconducting and normal states for deeply underdoped region [1, 2, 4, 7]. This result is surprising and contrasts the usual understanding of the d-wave superconducting pairing or the conventional pseudogap behavior; both should generate energy nodes along diagonal lines of the Brillouin zone. The opening of the nodal gap in the AF state is also intriguing. It was reported that the commensurate AF order forms at 140 K, well above the temperature that the nodal gap opens, which is only 45 K [6].

The above experimental observations challenge the present theory for high-T_c superconductors. As is known, even in the superconducting state the quasiparticle energy gap is not necessarily tied to the superconducting order parameter. It is rather important to explore the physics behind the gap-like feature. Previously, it was proposed that the spin-density-wave order may account for the nodal gap [8]. Recently many groups have attempted to give other possible theoretical scenarios for the nodal gap. It was proposed that the Coulomb disorder effects [9] or strong disordered magnetism [10] can account for the nodal gap while it was argued that the experimentally observed spectra are sufficiently sharp near the nodal momentum so that the nodal gap is unlikely disorder driven [2, 11]. Very recently, it was proposed that the underdoped high-T_c superconductors are topological superconductors and the topological phase is induced by the AF order. The nodal gap is due to an additional p-wave pairing term [11, 12] or d_{xy}-pairing term [13]. However, the existence of the AF order in the superconducting phase needs further experimental evidence. And so far there is no direct experimental observation to support

the p-wave or d_{xy} pairing component in high-T_c superconductors. Moreover, note that the nodal gap is also observed in the nonsuperconducting state [1–6]. It is temperature independent when crossing the superconducting transition temperature T_c [2]. This seems to suggest that the nodal gap is not superconductivity driven; thus the topological superconductivity scenario is challenged. Therefore, so far the origin for the nodal gap is still far from obvious and a widely accepted theoretical explanation is still awaited.

Actually, now our understanding of the underdoped high-T_c superconductors is still rather incomplete. There may exist various competing orders that can induce the gap-like feature. One possible candidate order is the spin order. Experimentally the presence of the spin order can be examined by neutron scattering experiments. It was reported that the incommensurate diagonal spin-density-wave order (ID-SDW) with the wave vectors $\mathbf{Q} = (\pi \pm \delta, \pi \pm \delta)$ forms in the deeply underdoped region [14–19]. As the doping density increases, the spin modulation along the parallel direction with the incommensurate wave vectors $(\pi, \pi \pm \delta)$ and $(\pi \pm \delta, \pi)$ was observed, accompanied by the appearance of the superconductivity. It was revealed that the diagonal spin order could persist in the superconducting state and coexist with the parallel spin order [18]. Very recently, based on the muon spin rotation measurement, the ID-SDW order was also observed in the AF state, with the temperature about 30 K. It is much lower than the AF Neel temperature, while it is close to that of the nodal gap being observed [6]. Therefore, the ID-SDW order and the nodal gap appear in the same region experimentally.

Motivated by the above experimental observations and theoretical attempts, and in order to give a more definitive explanation for the nodal gap, in the present work, we start from a phenomenological model in the presence of an ID-SDW order with the wave vectors $\mathbf{Q} = (\pi \pm \delta, \pi \pm \delta)$ to elaborate its effect on the spectral function. Our numerical results show that the nodal gap is reproduced in the presence of the above ID-SDW order. The numerical results are in good agreement with the experiments; thus we propose that the ID-SDW order is the main reason for the nodal gap. We also discuss the origin of the ID-SDW order and propose that it is understandable within the Fermi surface nesting picture. The renormalized Fermi surface in the normal state and the modulated real space local density of states are also calculated and the results are qualitatively consistent with previous experiments, which may be the additional evidences for the presence of the ID-SDW order. We also emphasize that our present theory is fundamentally different from previous one considering the existence of the static commensurate AF order [11–13]. Namely, in the present work, the superconducting pairing has always pure $d_{x^2-y^2}$ symmetry. The nodal gap will appear for even very weak ID-SDW order. It is induced directly by the spin order and would persist in the normal state.

Our starting phenomenological model includes the superconducting term and an ID-SDW order term, which is expressed as

$$H = H_{\mathrm{SC}} + H_S, \tag{1}$$

where the superconducting Hamiltonian is expressed as

$$H_{\mathrm{SC}} = -\sum_{\mathbf{ij},\sigma} t_{\mathbf{ij}} c^{\dagger}_{\mathbf{i}\sigma} c_{\mathbf{j}\sigma} - \mu \sum_{\mathbf{i}\sigma} c^{\dagger}_{\mathbf{i}\sigma} c_{\mathbf{i}\sigma} + \sum_{\mathbf{ij}} \left(\Delta_{\mathbf{ij}} c^{\dagger}_{\mathbf{i}\uparrow} c^{\dagger}_{\mathbf{j}\downarrow} + h.c. \right). \tag{2}$$

In the present work, we assume phenomenologically the SDW ordered periodically, expressed as

$$H_S = \sum_{\mathbf{iQ}_s} V_s S^z_{\mathbf{i}} e^{i\mathbf{R}_{\mathbf{i}}\cdot\mathbf{Q}_s}. \tag{3}$$

The above Hamiltonian can be transformed to the momentum space by taking into account the $d_{x^2-y^2}$-wave superconducting pairing, the nearest-neighbor, and next-nearest-neighbor hopping, which is rewritten as

$$H_{\mathrm{SC}} = \sum_{\mathbf{k}\sigma} \varepsilon_{\mathbf{k}} c^{\dagger}_{\mathbf{k}\sigma} c_{\mathbf{k}\sigma} + \sum_{\mathbf{k}} \left(\Delta_{\mathbf{k}} c^{\dagger}_{\mathbf{k}\uparrow} c^{\dagger}_{-\mathbf{k}\downarrow} + h.c. \right), \tag{4}$$

where $\varepsilon_{\mathbf{k}} = -2t(\cos k_x + \cos k_y) - 4t' \cos k_x \cos k_y - \mu$ and $\Delta_{\mathbf{k}} = \Delta_0(\cos k_x - \cos k_y)$. H_S is expressed as

$$H_S = \sum_{\mathbf{k}\sigma\mathbf{Q}_s} \left(V\sigma c^{\dagger}_{\mathbf{k}\sigma} c_{\mathbf{k}+\mathbf{Q}_s,\sigma} + h.c. \right), \tag{5}$$

with $V = V_s/2$ being the ID-SDW order magnitude.

In the present work, we consider the four incommensurate scattering wave vectors $\mathbf{Q}_s = (\pi \pm \delta, \pi \pm \delta)$, consistent with previous experiments [6, 14–19]. Hereafter, if not specified otherwise, the parameters are used as $t = 1, t' = -0.3$, $\mu = -0.857$ (corresponding to the doping $x = 0.08$), $\Delta_0 = 0.25$, and $V = 0.1$. The incommensurability δ is taken as 0.15π, which is obtained from the Fermi surface nesting vector, as discussed below. We have checked numerically that our results are not sensitive to the reasonable changes of the chosen parameters.

Before presenting our results, let us elaborate the numerical technique with the incommensurate order. Firstly one may rewrite the Hamiltonian to the matrix form with the basis including the particle operator $c_{\mathbf{k}\sigma}$ and $c_{\mathbf{k}+n\mathbf{Q}_s,\sigma}$ ($n = 1, 2, 3, \ldots$). For commensurate density wave (e.g., $\mathbf{Q}_s = (2s\pi/N, 0)$), the wave vectors $\mathbf{k}$ and $\mathbf{k} + N\mathbf{Q}_s$ have the same reduced wave vectors in the first Brillouin zone. As a result, the Hamiltonian is expressed as a finite order matrix and can be solved strictly. However, for incommensurate density-wave order with irrational real space modulation, the order of the Hamiltonian matrix is indeed infinite and can only be solved approximately. Since generally the incommensurability is usually considered approximately as a finite decimal, then the Hamiltonian can be solved numerically. For the present incommensurability under consideration ($\delta = 0.15\pi = 2\pi * 3/40$), the whole Brillouin zone is divided into $40 \times 40 = 1600$ parts. The Hamiltonian with the superconducting pairing can be written as 3200×3200 matrix. Then the retarded Green's function $G(\mathbf{k}, \omega + i\Gamma)$ can be obtained through diagonalizing the Hamiltonian. The quasiparticle spectral function $A(\mathbf{k}, \omega)$ is given from

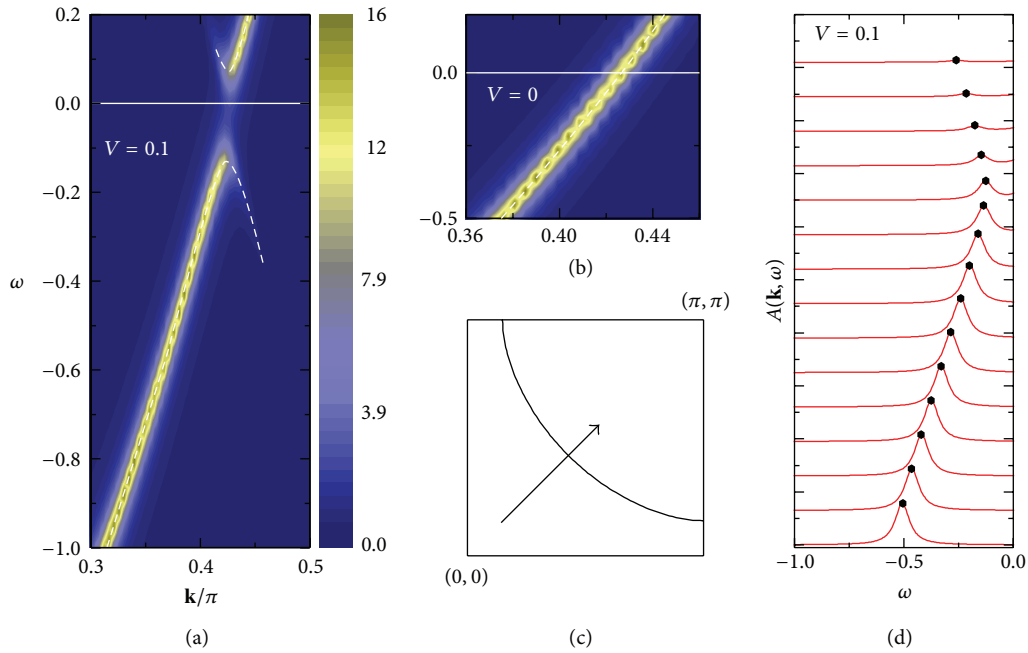

FIGURE 1: ((a)-(b)) Intensity plots of the spectral function with and without the ID-SDW order, respectively. (c) The normal state Fermi surface. The arrow indicates the cut along which (a), (b), and (d) were taken. (d) The energy dependence of the spectral function along the arrow in (c) (from bottom to top).

the retarded Green's function with $A(\mathbf{k}, \omega) = -\operatorname{Im} G(\mathbf{k}, \omega + i\Gamma)/\pi$.

We show in Figures 1(a) and 1(b) the spectral function along the diagonal direction (along the cut indicated in Figure 1(c)) with and without the ID-SDW order, respectively. The dashed lines are the quasiparticle dispersions. The spectral functions as a function of the energy (EDCs) along the diagonal direction are plotted in Figure 1(d). As is seen, the quasiparticle energy decreases as the wave vector moves towards the Fermi surface. An obvious gap exists in the presence of the ID-SDW order, as shown in Figure 1(a). We can also see clearly that the gap closes and the quasiparticle dispersion crosses the Fermi momentum K_F for $V = 0$, as is seen in Figure 1(b). We also checked numerically that the above results are in fact independent of the d-wave pairing magnitude Δ_0 and the nodal gap exists when we set $\Delta_0 = 0$ (not shown here). Therefore, the above nodal gap should exist both in the superconducting state and the normal state. Our results for the nodal gap are qualitatively consistent with the experiments [1–7].

The momentum dependence of the energy gap along the Fermi surface is studied in Figure 2. The EDCs with different Fermi surface angle θ (defined in Figure 2(b)) are plotted in Figure 2(a). We define the energy gaps as the peak positions of EDCs. Then the energy gap as a function of the Fermi angle is shown in Figure 2(c). As is seen, the energy gap is significantly anisotropic. It reaches the maxima value at the Brillouin boundary and decreases when the wave vector moves towards the diagonal direction. It reaches the minimum value at the diagonal direction. The d-wave gap magnitude is also plotted in Figure 2(c) for comparison. The observed energy gap and the d-wave gap are nearly the same near the antinodal direction. Near the diagonal direction the gap is different from the d-wave one; namely, an obvious finite gap exists due to the presence of the ID-SDW order. The above results are qualitatively consistent with the experimental observations in the superconducting state [2]. Note that here the wave vector $\mathbf{Q}$ is important for the momentum dependence of the energy gap. We also note that very recent ARPES experiment on the insulating samples has also revealed that the energy gap is anisotropic; that is, it reaches the maxima value at the Brillouin zone boundary and is minimum at the diagonal direction [5]. This experimental result can also be explained qualitatively based on our model. Note that the origin of the energy gap in deeply underdoped high-T_c materials is indeed complicated. There may exist several candidate competing orders. We propose that the energy gap near the d-wave nodal points is still due to the ID-SDW order. The gap near the Brillouin boundary is generated by another order (e.g., the d-density wave order [20] or the AF order (at the mean-field level, the AF order can be obtained simply by setting $\mathbf{Q}_s = (\pi; \pi)$ in (5))). The coexistence of two orders in the insulating sample is also supported by very recent experiments [6]. Theoretically, the energy gap produced by the d-density-wave order or AF order should be maximum near the hot spots (the crossing points between the normal state Fermi surface and the magnetic Brillouin zone). For hole doped samples, the hot spots are close to the antinodal points. Thus the anisotropic gap in nonsuperconducting materials [5] is understandable. We have also checked numerically (not shown here) that

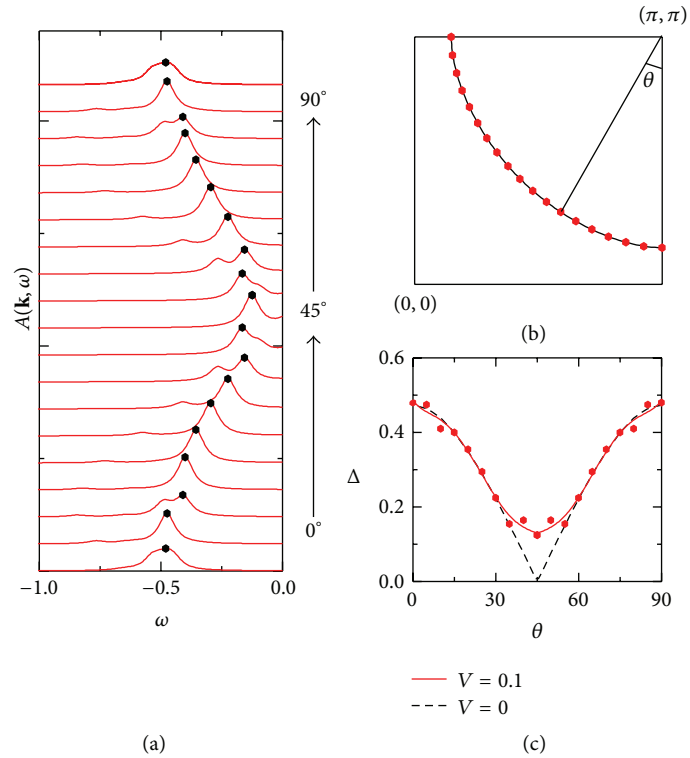

FIGURE 2: (a) The energy dependence of the spectral functions for different Fermi angle θ, with the points and the Fermi angle being shown in (b). (c) The energy gap as a function of the Fermi angle. The closed circles are the energy gap obtained from (a). The red solid line is a polynomial fitting for the data. The dashed line is the d-wave superconducting gap magnitude.

similar anisotropic behavior can be reproduced with the model including both the ID-SDW order and the d-density-wave order (or the AF order).

The explanation of the ID-SDW order can be given based on the Fermi surface nesting picture. The normal state Fermi surface is shown in Figure 3. As is seen, the tangent lines of the Fermi surface curve are parallel at the d-wave nodal points, revealing the Fermi surface nesting feature. The corresponding nesting vector is marked in Figure 3, for which the incommensurability can be obtained from the Fermi momentum along the diagonal direction. The ID-SDW order comes mainly from such node-to-node excitations. As such, the existence of the nodal gap can be immediately understood. Namely, the vector of the ID-SDW order connects different nodal points of Fermi surface. The electron hopping between these points can occur due to the ID-SDW order. This destroys the state of the quasiparticle near nodal points and an energy gap opens.

We now discuss the differences between our model and previous one in [8]. A commensurate SDW order with the wave vector (π, π) was taken into account in [8]. For the ID-SDW order considered in our present work, the SDW gap is opened first at the nodal direction, while, for the commensurate SDW order, the SDW gap is opened first near the antinodal direction and the nodal gap appears for a relatively strong SDW order. As a result, the momentum space of the total energy gap (shown in Figure 2) may be different as the SDW wave vector changes to the commensurate one.

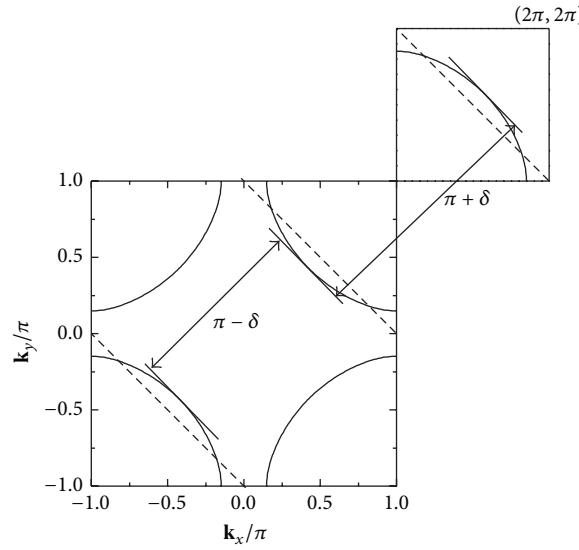

FIGURE 3: The normal state Fermi surface ($\varepsilon_{\mathbf{k}} = 0$). The diagonal nesting wave vectors are indicated.

The signatures of this ID-SDW order can be probed by studying the normal state Fermi surface. Previously many interesting results for the Fermi surface of underdoped cuprates have been obtained by ARPES experiments. One important observation is that the Fermi surface is

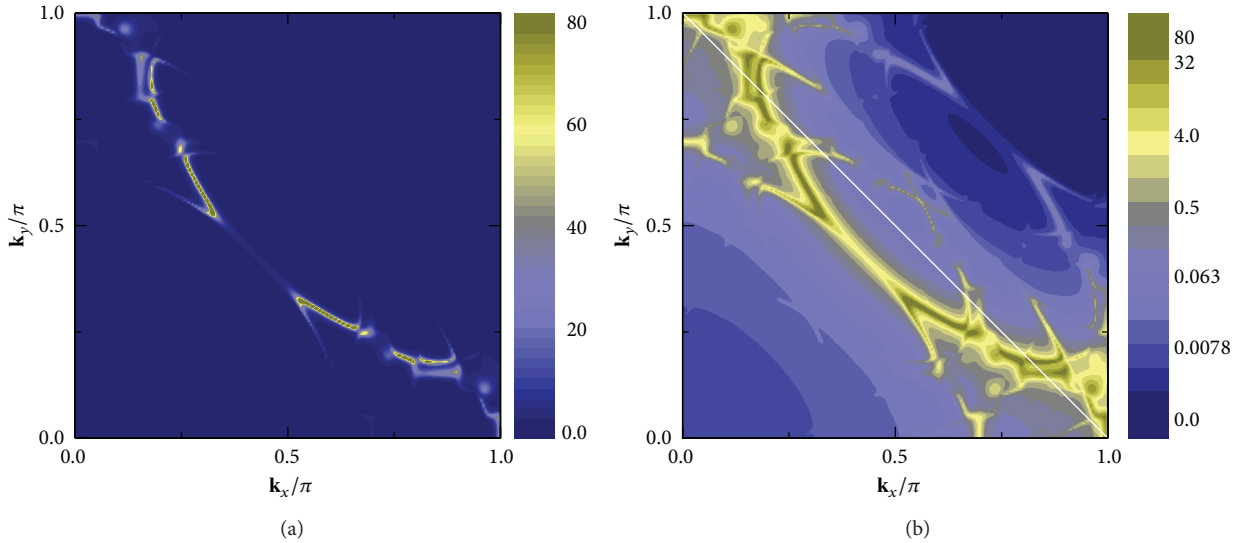

FIGURE 4: (a) The intensity plot of the zero energy spectral function $A(\mathbf{k}, \omega = 0)$ with $\Delta_0 = 0$ and $V = 0.1$. (b) The same as (a) while the logarithmic scale is used.

gapped near the antinodal direction and leaves an ungapped Fermi arc [21]. This conventional pseudogap behavior is still unsolved and not concerned with in the present work. On the other hand, the electronic structure along diagonal direction is also nontrivial. It was revealed that the spectral weight is low and the quasiparticle peak is broad near the nodal direction for underdoped $La_{2-x}Sr_xCuO_4$ samples [22, 23]. Another interesting result is the observation of the Fermi pocket in the underdoped samples [24]. It was revealed that the Fermi pocket coexists with the Fermi arc and exists only in the underdoped samples. Interestingly, the experimentally observed Fermi pocket is not symmetrical with respect to the $(0, \pi)$ to $(\pi, 0)$ line. Thus the d-density-wave order or AF order may not account for the Fermi pocket. It was also proposed in [24] that the incommensurate diagonal density-wave may potentially explain their results.

The numerical results of the normal state zero energy spectral function $[A(\mathbf{k}, \omega = 0)]$ ($\Delta_0 = 0$, $V = 0.1$) is presented in Figure 4. The normal state Fermi surface can be obtained through the peaks of the spectral function. As is seen in Figure 4(a), the spectral weight near the diagonal direction is quite low, consistent with the experimental observations [22, 23]. This is due to the node-to-node scattering caused by the ID-SDW. When the spectral function is plotted in a logarithmic scale, the weak features of the spectral function are revealed more clearly. As is seen, besides the main Fermi surface, contributed by the normal state energy band $\varepsilon_{\mathbf{k}}$, another band with much lower spectral weight can be seen clearly. Then a Fermi pocket forms. Here the Fermi pocket is nonsymmetrical and not centered at $(\pi/2, \pi/2)$. The above results are qualitatively consistent with the recent experimental observation [24].

The relationship of the SDW and charge-density-wave (CDW) orders has been an important point and attracted intensive attention previously. Experimentally the charge order could be detected through the STM experiments. One prominent feature is the "checkerboard structure" from the energy-dependent local density of states (LDOS). It was first reported to exist in vortex cores of optimally doped materials, with a two-dimensional modulation along Cu–O bond directions [25–27]. Later experiments also observed similar modulation in the superconducting samples without the magnetic field [28, 29]. In the meantime, the charge order can also be revealed in more detail through the Fourier transform of the LDOS (FT-LDOS). The nondispersive peaks would be observed in the presence of the charge modulation. The periodicity can be determined through the peak positions in the momentum space. An incommensurate charge modulation with the periodicity of about $4.5a$~$4.7a$ was reported in the normal and superconducting states [30–32].

We now study numerically the real space modulation induced by the ID-SDW order. Diagonalizing the Hamiltonian (1), we can obtain the LDOS $\rho(\mathbf{i}, \omega)$ numerically. To compare with the STM experiments, we also define the Fourier transformation of the LDOS (FT-LDOS), which is expressed as $Z(\mathbf{q}, \omega) = \sum_{\mathbf{i}} \rho_{\mathbf{i}}(\omega) \exp(i\mathbf{R}_{\mathbf{i}} \cdot \mathbf{q})$. The numerical results for the LDOS and FT-LDOS are presented in Figure 5. The LDOS in the normal state with the energy $\omega = 0.1$ is plotted in Figure 5(a). The checkerboard pattern is revealed clearly. Figure 5(b) is the FT-LDOS spectra. There exist four peaks at the wave vector $(0, \pm 0.3\pi)$ and $(\pm 0.3\pi, 0)$ (indicated with circles). The above results are robust and qualitatively the same for different energies. The LDOS and FT-LDOS in the superconducting state are plotted in Figures 5(c) and 5(d). As is seen, the intensities decrease due to the existence of the superconducting gap while the main results are qualitatively the same as those of the normal state. Interestingly, although here we consider the ID-SDW order in the starting model, the modulations of LDOS are along the Cu–O bond directions. This is consistent with the STM observations. It is also worthwhile to point out that

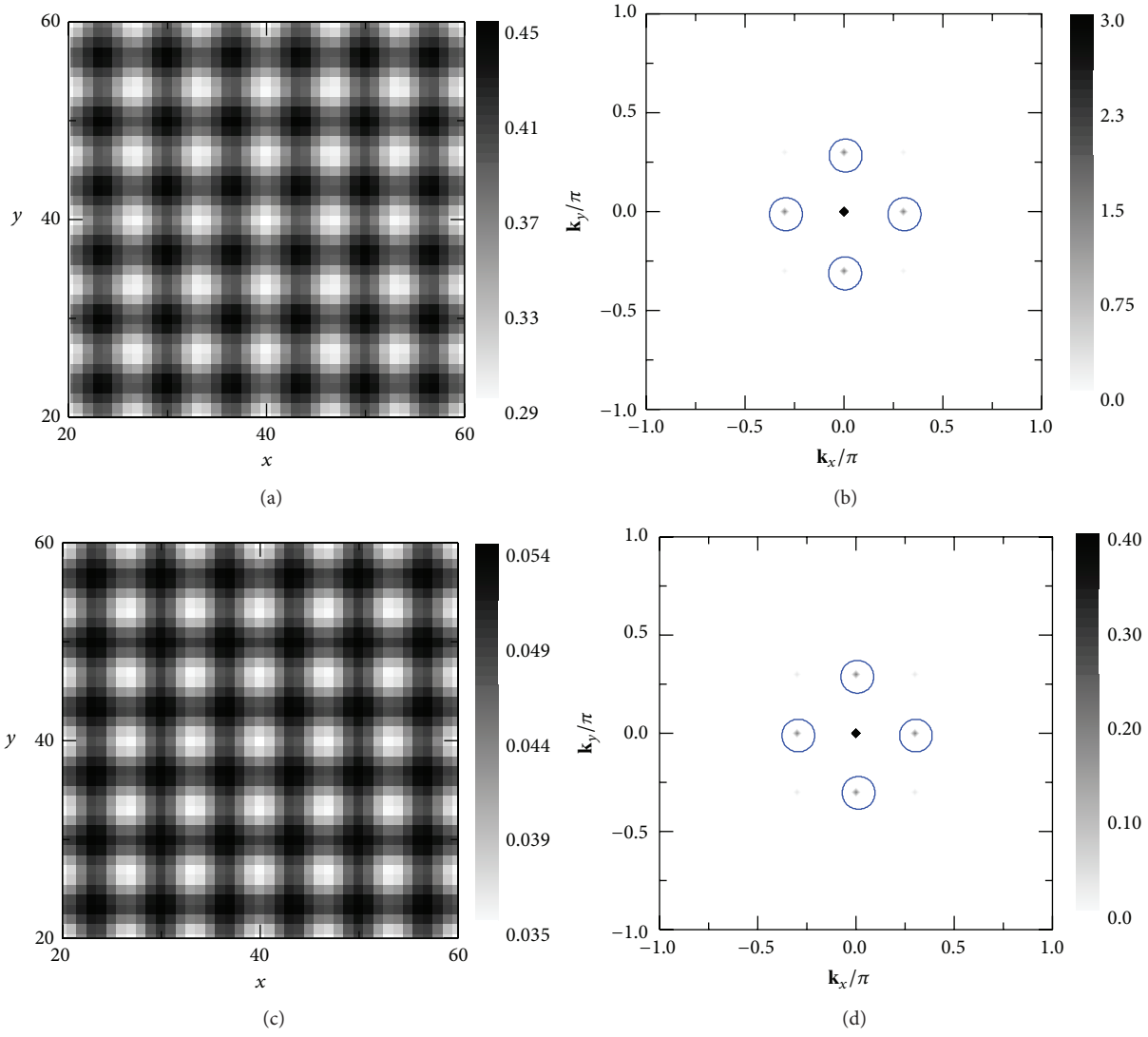

FIGURE 5: The LDOS $[\rho_i(\omega)]$ and FT-LDOS $[Z(\mathbf{q}, \omega)]$ in the normal state and superconducting state with $V = 0.1$ and $\omega = 0.1$. (a) LDOS in the normal state with $\Delta = 0$. (b) FT-LDOS in the normal state. (c) LDOS in the superconducting state with $\Delta_0 = 0.25$. (d). FT-LDOS in the superconducting state.

the relation between the SDW order and charge order is still an open question. If both have the same origins, then a simple relation for the incommensurability of the SDW order δ_s and the CDW order δ_c should satisfy $\delta_c = 2\delta_s$ [33]. Experimentally this relation is consistent with the observations in $La_{2-x}Sr_xCuO_4$ [33, 34] and $La_{2-x}Ba_xCuO_4$ [35] samples. However, it was also revealed that this relation is not satisfied in the $Bi_2Sr_{2-z}La_zCuO_{6+x}$ [36, 37] and $YBa_2Cu_3O_y$ samples [38].

In summary, based on a phenomenological model, we elaborate that an ID-SDW order can cause a finite gap along the d-wave nodal line. This is in good agreement with recent experimental observations. The origin of the ID-SDW order can be explained through the Fermi surface nesting picture. The normal state Fermi surface and the local density of states are also studied. The results are qualitatively consistent with the experiments.

Conflict of Interests

The authors declare that there is no conflict of interests regarding the publication of this paper.

Acknowledgments

This work was supported by the NSFC (Grants nos. 11374005 and 11204138), the NCET (Grant no. NCET-12-0626), NSF of Jiangsu Province of China (Grant no. BK2012450), Jiangsu Qingnan Engineering project, and U.S. DOE Office of Basic Energy Sciences.

References

[1] J. W. Harter, L. Maritato, D. E. Shai et al., "Nodeless superconducting phase arising from a strong (π, π) antiferromagnetic

phase in the infinite-layer electron-doped $Sr_{1-x}La_xCuO_2$ compound," *Physical Review Letters*, vol. 109, Article ID 267001, 2012.

[2] I. M. Vishik, M. Hashimoto, R.-H. He et al., "Phase competition in trisected superconducting dome," *Proceedings of the National Academy of Sciences of the United States of America*, vol. 109, pp. 18332–18337, 2012.

[3] T. Valla, "Angle-resolved photoemission from cuprates with static stripes," *Physica C*, vol. 481, pp. 66–74, 2012.

[4] E. Razzoli, G. Drachuck, A. Keren et al., "Evolution from a nodeless gap to $dx_2 - y_2$-wave in underdoped $La_{2-x}Sr_xCuO_4$," *Physical Review Letters*, vol. 110, no. 4, Article ID 047004, 5 pages, 2013.

[5] Y. Peng, J. Meng, D. Mou et al., "Disappearance of nodal gap across the insulator–superconductor transition in a copper-oxide superconductor," *Nature Communications*, vol. 4, article 2459, 2013.

[6] G. Drachuck, E. Razzoli, G. Bazalitski et al., "Comprehensive study of the spin-charge interplay in antiferromagnetic $La_{2-x}Sr_xCuO_4$," *Nature Communications*, vol. 5, article 3390, 2014.

[7] K. M. Shen, T. Yoshida, D. H. Lu et al., "Fully gapped single-particle excitations in lightly doped cuprates," *Physical Review B*, vol. 69, Article ID 054503, 2004.

[8] Z. Nazario and D. I. Santiago, "Coexistence of spin-density wave and D-wave superconducting order parameter," *Physical Review B*, vol. 70, no. 14, Article ID 144513, 2004.

[9] W. Chen, G. Khaliullin, and O. P. Sushkov, "Coulomb disorder effects on angle-resolved photoemission and nuclear quadrupole resonance spectra in cuprates," *Physical Review B*, vol. 80, no. 9, Article ID 094519, 2009.

[10] W. A. Atkinson, J. D. Bazak, and B. M. Andersen, "Robust nodal *d*-wave spectrum in simulations of a strongly fluctuating competing order in underdoped cuprate superconductors," *Physical Review Letters*, vol. 109, Article ID 267004, 2012.

[11] Y.-M. Lu, T. Xiang, and D.-H. Lee, "Underdoped superconducting cuprates as topological superconductors," *Nature Physics*, vol. 10, no. 9, pp. 634–637, 2014.

[12] T. Das, "Nodeless superconducting gap induced by a competing odd-parity Fulde-Ferrel-Larkin-Ovchinnikov superconductivity in deeply underdoped cuprates," http://arxiv.org/abs/1312.0544.

[13] A. Gupta and D. Sa, "Topological phases due to the coexistence of superconductivity and spin-density wave: application to high Tc superconductors in the underdoped regime," http://arxiv.org/abs/1401.0617.

[14] S. Wakimoto, G. Shirane, Y. Endoh et al., "Observation of incommensurate magnetic correlations at the lower critical concentration for superconductivity in $La_{2-x}Sr_xCuO_4(x = 0.05)$," *Physical Review B*, vol. 60, article R769, 1999.

[15] S. Wakimoto, R. J. Birgeneau, M. A. Kastner et al., "Direct observation of a one-dimensional static spin modulation in insulating $La_{1.95}Sr_{0.05}CuO_4$," *Physical Review B*, vol. 61, no. 5, pp. 3699–3706, 2000.

[16] M. Matsuda, M. Fujita, K. Yamada et al., "Static and dynamic spin correlations in the spin-glass phase of slightly doped $La_{2-x}Sr_xCuO_4$," *Physical Review B*, vol. 62, no. 13, pp. 9148–9154, 2000.

[17] S. Wakimoto, J. M. Tranquada, T. Ono et al., "Diagonal static spin correlation in the low-temperature orthorhombic Pccn phase of $La_{1.55}Nd_{0.4}Sr_{0.05}CuO_4$," *Physical Review B*, vol. 64, Article ID 174505, 2001.

[18] M. Fujita, K. Yamada, H. Hiraka et al., "Static magnetic correlations near the insulating-superconducting phase boundary in $La_{2-x}Sr_xCuO_4$," *Physical Review B*, vol. 65, Article ID 064505, 2002.

[19] M. Enoki, M. Fujita, T. Nishizaki et al., "Spin-stripe density varies linearly with the hole content in single-layer $Bi_{2+x}Sr_{2-x}CuO_{6+y}$ cuprate superconductors," *Physical Review Letters*, vol. 110, Article ID 017004, 2013.

[20] S. Chakravarty, R. B. Laughlin, D. K. Morr, and C. Nayak, "Hidden order in the cuprates," *Physical Review B*, vol. 63, no. 9, Article ID 094503, 2001.

[21] T. Timusk and B. Statt, "The pseudogap in high-temperature superconductors: an experimental survey," *Reports on Progress in Physics*, vol. 62, no. 1, pp. 61–122, 1999.

[22] A. Ino, C. Kim, T. Mizokawa et al., "Fermi surface and band dispersion in $La_{2-x}Sr_xCuO_4$," *Journal of the Physical Society of Japan*, vol. 68, pp. 1496–1499, 1999.

[23] A. Ino, C. Kim, M. Nakamura et al., "Electronic structure of $La_{2-x}Sr_xCuO_4$ in the vicinity of the superconductor-insulator transition," *Physical Review B*, vol. 62, no. 6, pp. 4137–4141, 2000.

[24] J. Meng, G. Liu, W. Zhang et al., "Coexistence of Fermi arcs and Fermi pockets in a high-T_c copper oxide superconductor," *Nature*, vol. 462, no. 7271, pp. 335–338, 2009.

[25] J. E. Hoffman, E. W. Hudson, K. M. Lang et al., "A four unit cell periodic pattern of quasi-particle states surrounding vortex cores in $Bi_2Sr_2CaCu_2O_8+\delta$," *Science*, vol. 295, no. 5554, pp. 466–469, 2002.

[26] J.-X. Zhu and C. S. Ting, "Quasiparticle states at a *d*-wave vortex core in high- T_c superconductors: induction of local spin density wave order," *Physical Review Letters*, vol. 87, Article ID 147002, 2001.

[27] J.-X. Zhu, I. Martin, and A. R. Bishop, "Spin and charge order around vortices and impurities in high-Tc superconductors," *Physical Review Letters*, vol. 89, no. 6, Article ID 067003, 2002.

[28] C. Howald, H. Eisaki, N. Kaneko, M. Greven, and A. Kapitulnik, "Periodic density-of-states modulations in superconducting $Bi_2Sr_2CaCu_2O_{8+\sigma}$," *Physical Review B*, vol. 67, no. 1, Article ID 14533, 2003.

[29] T. Hanaguri, C. Lupien, Y. Kohsaka et al., "A 'checkerboard' electronic crystal state in lightly hole-doped $Ca_{2-x}Na_xCuO_2Cl_2$," *Nature*, vol. 430, pp. 1001–1005, 2004.

[30] M. Vershinin, S. Misra, S. Ono, Y. Abe, Y. Ando, and A. Yazdani, "Local ordering in the pseudogap state of the high-T_c superconductor $Bi_2Sr_2CaCu_2O_{8+\delta}$," *Science*, vol. 303, no. 5666, pp. 1995–1998, 2004.

[31] A. Fang, C. Howald, N. Kaneko, M. Greven, and A. Kapitulnik, "Periodic coherence-peak height modulations in superconducting $Bi_2Sr_2CaCu_2O_{8+\delta}$," *Physical Review B—Condensed Matter and Materials Physics*, vol. 70, no. 21, Article ID 214514, pp. 1–8, 2004.

[32] K. McElroy, D.-H. Lee, J. E. Hoffman et al., "Coincidence of checkerboard charge order and antinodal state decoherence in strongly underdoped superconducting $Bi_2Sr_2CaCu_2O_{8+\delta}$," *Physical Review Letters*, vol. 94, no. 19, Article ID 197005, 4 pages, 2005.

[33] J. M. Tranquada, B. J. Sternlieb, J. D. Axe, Y. Nakamura, and S. Uchida, "Evidence for stripe correlations of spins and holes in copper oxide superconductors," *Nature*, vol. 375, no. 6532, pp. 561–563, 1995.

[34] T. P. Croft, C. Lester, M. S. Senn, A. Bombardi, and S. M. Hayden, "Charge density wave fluctuations in $La_{2-x}Sr_xCuO_4$

and their competition with superconductivity," *Physical Review B*, vol. 89, Article ID 224513, 2014.

[35] M. Hücker, M. V. Zimmermann, G. D. Gu et al., "Stripe order in superconducting $La_{2-x}Ba_xCuO_4(0.095 \leq x \leq 0.155)$," *Physical Review B*, vol. 83, Article ID 104506, 2011.

[36] W. D. Wise, M. C. Boyer, K. Chatterjee et al., "Charge-density-wave origin of cuprate checkerboard visualized by scanning tunnelling microscopy," *Nature Physics*, vol. 4, pp. 696–699, 2008.

[37] R. Comin, A. Frano, M. M. Yee et al., "Charge order driven by fermi-arc instability in $Bi_2Sr_{2-x}La_xCuO_{6+\delta}$," *Science*, vol. 343, no. 6169, pp. 390–392, 2014.

[38] E. Blackburn, J. Chang, M. Hücker et al., "X-ray diffraction observations of a charge-density-wave order in superconducting ortho-II $YBa_2Cu_3O_{6.54}$ single crystals in zero magnetic field," *Physical Review Letters*, vol. 110, Article ID 137004, 2013.

Hindawi Publishing Corporation
Advances in Condensed Matter Physics
Volume 2015, Article ID 605160, 5 pages
http://dx.doi.org/10.1155/2015/605160

Research Article

Inelastic Neutron Scattering Studies on the Crystal Field Excitations in Superconducting $NdFeAsO_{0.85}F_{0.15}$

Peng Cheng,[1] Wei Bao,[1] Sergey Danilkin,[2] Tiesong Zhao,[1] Jieming Sheng,[1] Juanjuan Liu,[1] Wei Luo,[1] and Jinchen Wang[1]

[1]*Department of Physics, Renmin University of China, Beijing 100872, China*
[2]*Bragg Institute, Australian Nuclear Science and Technology Organization, Locked Bag 2001, Kirrawee DC, NSW 2232, Australia*

Correspondence should be addressed to Peng Cheng; pcheng@ruc.edu.cn

Received 7 December 2014; Revised 26 February 2015; Accepted 2 March 2015

Academic Editor: Viorel Sandu

Inelastic neutron scattering experiments were performed on polycrystalline samples of $NdFeAsO_{0.85}F_{0.15}$ over a wide temperature range (3 K–250 K). Based on the analysis of the experimental data, a Nd^{3+} CF energy level scheme is proposed to give a consistent explanation about the observed CF transitions. The observed extra ground-state CF transitions could not be simply explained by the transitions between five Kramers doublets split from the Nd^{3+} $^4I_{9/2}$ ground state in the C_{4v} point symmetry. A reliable explanation would be a superposition of crystal fields due to different local symmetries around the Nd^{3+} ions induced by the fluorine doping.

1. Introduction

For materials with rare-earth (R) elements, the interactions between f-electrons and the crystal field potentials produced by local lattice environment play important roles in determining the electronic ground state of R ions, as well as in understanding the magnetic and thermodynamic properties of these compounds. Inelastic neutron scattering has been widely accepted as the most reliable technique in determining the crystal field potentials in rare-earth based materials. Particularly, for superconducting materials, in either high-T_c cuprates or other R based heavy fermion superconductors, important research progress has been made in investigating the neutron spectroscopy of the CF excitations [1, 2].

The discovery of Fe-based superconductor LaFe AsO_{1-x} F_x has caused a tremendous upsurge of scientific interest since 2008 [3]. Shortly after the report of 26 K superconductivity in $LaFeAsO_{1-x}F_x$, through the substitution of La by other R elements with f-electrons (such as Ce, Pr, Nd, and Sm), superconducting critical temperature T_c above 50 K could be observed in $RFeAsO_{1-x}F_x$ [4–6]. So far, these so-called FeAs-1111 compounds mark the highest T_c in all Fe-based superconductors, which also provided a unique opportunity in studying the correlation between CF excitations and physical properties in these exotic superconducting families. Up to now, there have been several publications about crystal field studies in FeAs-1111 compounds through inelastic neutron scattering technique. For example, in $CeFeAsO_{1-x}F_x$ ($x = 0, 0.16$), the Ce CF levels were determined and the intrinsic linewidth Γ of 18.7 meV was found to have a clear anomaly at T_c [7]; inelastic neutron scattering measurements of CF transitions in $RFeAsO_{1-x}F_x$ (RE = Pr, Nd) provided evidences that there were two distinct charge environments around the RE ions arising from a random distribution of fluorine ions [8]. The CF level structures for both paramagnetic phase and antiferromagnetic phase of NdFeAsO were constructed by Xiao et al. [9]. However, for $NdFeAsO_{1-x}F_x$, there are still insufficient neutron scattering data on the CF transitions and the CF energy level scheme of Nd ion is still not clear.

In this paper, we report inelastic neutron scattering studies on superconducting $NdFeAsO_{0.85}F_{0.15}$ samples. Based on the analysis of inelastic neutron scattering spectra at different temperatures, we propose a crystal field energy level scheme for Nd ion, which could explain the CF transitions observed in the experimental data. The additional CF transitions beyond the requirements of C_{4v} point symmetry indicate the superposition of crystal field

and inhomogeneous ligand environments around the rare-earth ions in $NdFeAsO_{0.85}F_{0.15}$.

2. Experimental Results and Discussions

About 20 grams of $NdFeAsO_{0.85}F_{0.15}$ polycrystalline samples were synthesized using the solid state reaction method. Resistivity measurements show that the onset superconducting transition temperature of our samples is about 47 K while the state of zero resistivity is reached at about 43 K, as shown in the inset of Figure 1(a). Inelastic neutron scattering measurements on $NdFeAsO_{0.85}F_{0.15}$ were carried out on thermal triple-axis spectrometer TAIPAN at the Australian research reactor OPAL [10]. The final neutron energy E_f was set to be 14.7 meV, with pyrolytic graphite (PG) as the monochromator and analyzer. The collimation was 48′-40′-40′-120′.

Figure 1 shows the raw data of the inelastic neutron spectra for $NdFeAsO_{0.85}F_{0.15}$ at different temperatures. From 3 K to 250 K, constant-Q scans were performed every 50 Kelvin. The momentum transfer Q was fixed to be 3.1 Å in the whole measurements. First of all, the strong peaks at about 45 meV and 40 meV (marked with red stars) could be easily distinguished as the spurious peaks, which originated from the 2λ elastic neutron scattering. (The best energy windows for PG filter are 14.7 meV and 13.5 meV. In our experimental setup, E_f was fixed to be 14.7 meV; when E_i = 58.8 meV and 54 meV, the energy transfers of 2λ neutron (14.7 meV and 13.5 meV) were corresponding to the strong elastic scattering signals. That is the origin of the spurious peaks at the energy transfers equaling 44.1 meV and 40.5 meV.) At below 30 meV plenty of CF excitation peaks could be clearly observed in the spectra at 3 K (marked with green arrows). With increasing temperature, the intensities of these peaks gradually decreased, which indicates that the corresponding CF excitations are ground-state excitations. In high temperature regions, some new CF peaks gradually emerge at around 11 meV and their absolute intensities got higher with increasing temperature. So these peaks should correspond to the excitations between excited CF states.

In order to fit and carefully analyze the CF peaks, after subtracting the spurious peaks, the next thing needed is to clarify the phonon contributions from the inelastic neutron spectrum. From both experimental data and theoretical calculations, it is known that the phonon spectra are almost the same for both parent compound and F-doped superconductors in FeAs-1111 system [11–13]. So with the generalized phonon density of states (GDOS) of NdFeAsO in reference paper [9], after transformation with Bose factor and the neutron cross section equation [14, 15]

$$\frac{d^2\sigma}{d\Omega\, dE} = N\frac{k_f}{k_i}\frac{(\gamma r_0)^2}{4} g_J^2 S(Q,E), \quad (1)$$

we can finally calculate the phonon background for each temperature in our inelastic neutron spectra. The results calculated for T = 3 K are shown in Figure 1(f) (red hollow scatters).

After subtracting phonons, we noticed that the spectrum at 3 K almost overlaps with the spectrum at high temperatures in energy transfer above 36 meV except for notable additional intensity contributions between 40 meV and 48 meV. These additional neutron intensities gradually disappeared with increasing temperatures, which indicates the existence of ground-state CF excitations in this energy range. So it is reasonable to choose the spectrum above 36 meV at high temperature as instrument background because these intensities could not come from CF excitations and most likely result from the 2λ neutron contributions. After subtracting both the phonon and instrument background, the spectrum obtained at 3 K could be well fitted by seven CF excitation peaks with the method of Gaussian fitting, as shown in Figure 2(a) (labelled as A–G, resp.). The similar crystal field excitations at energy transfer below 30 meV were also observed by Goremychkin et al. [8]. Because our data included higher energy transfer region, we could observe the CF excitations at 41.5 meV and 44.5 meV. From both Figures 1 and 2(b), it can be seen that the intensities of all these seven CF peaks decrease with increasing temperatures, which is clearly the characteristic of ground-state excitations.

Therefore based on our inelastic neutron data, we proposed a Nd^{3+} CF energy level scheme for $NdFeAsO_{0.85}F_{0.15}$, which is illustrated in Figure 3. The crystal field energy levels of NdFeAsO were obtained from another publication [9]. As shown in Figure 3, under crystal field with the C_{4v} point symmetry, the Nd^{3+} $^4I_{9/2}$ ground state splits into five doublets in NdFeAsO at temperatures above the antiferromagnetic and structural phase transition [9]. For $NdFeAsO_{0.85}F_{0.15}$, the ground-state CF transitions marked as "A" to "G" in Figure 3 were observed in the inelastic neutron spectra as shown in both Figures 1 and 2(a). From the comparison between the 150 K and 3 K data in Figure 2(b), we could also notice that, in high temperature neutron spectra, there were some new CF peaks emerging at around 11 meV and 26 meV. These new CF peaks were corresponding to the excitations between excited states, as illustrated in Figure 3 (i.e., transitions "H" and "I"). The consistence between the observed CF transitions and the CF energy level scheme proved the validity of our CF model proposed in this paper.

It is clear that the CF level scheme of $NdFeAsO_{0.85}F_{0.15}$ is significantly different from that of tetragonal NdFeAsO. In order to understand this difference, first of all we need to check whether there were CF states splitting caused by magnetic phase transitions. In the inset of Figure 1(a), the typical temperature dependence of resistances was measured on our samples. There were no traces of phase transitions because there was no anomaly in the normal state resistance which should be the typical features in the samples with structural or magnetic phase transitions. The resistance measurements were also performed in different batches of our samples which show similar features. Also based on our previous neutron measurements on samples with similar doping [16], we could safely rule out the possibility of structural or magnetic phases transitions induced additional CF states.

All the CF peaks should correspond to certain transitions of Nd f-electrons between different CF states. In

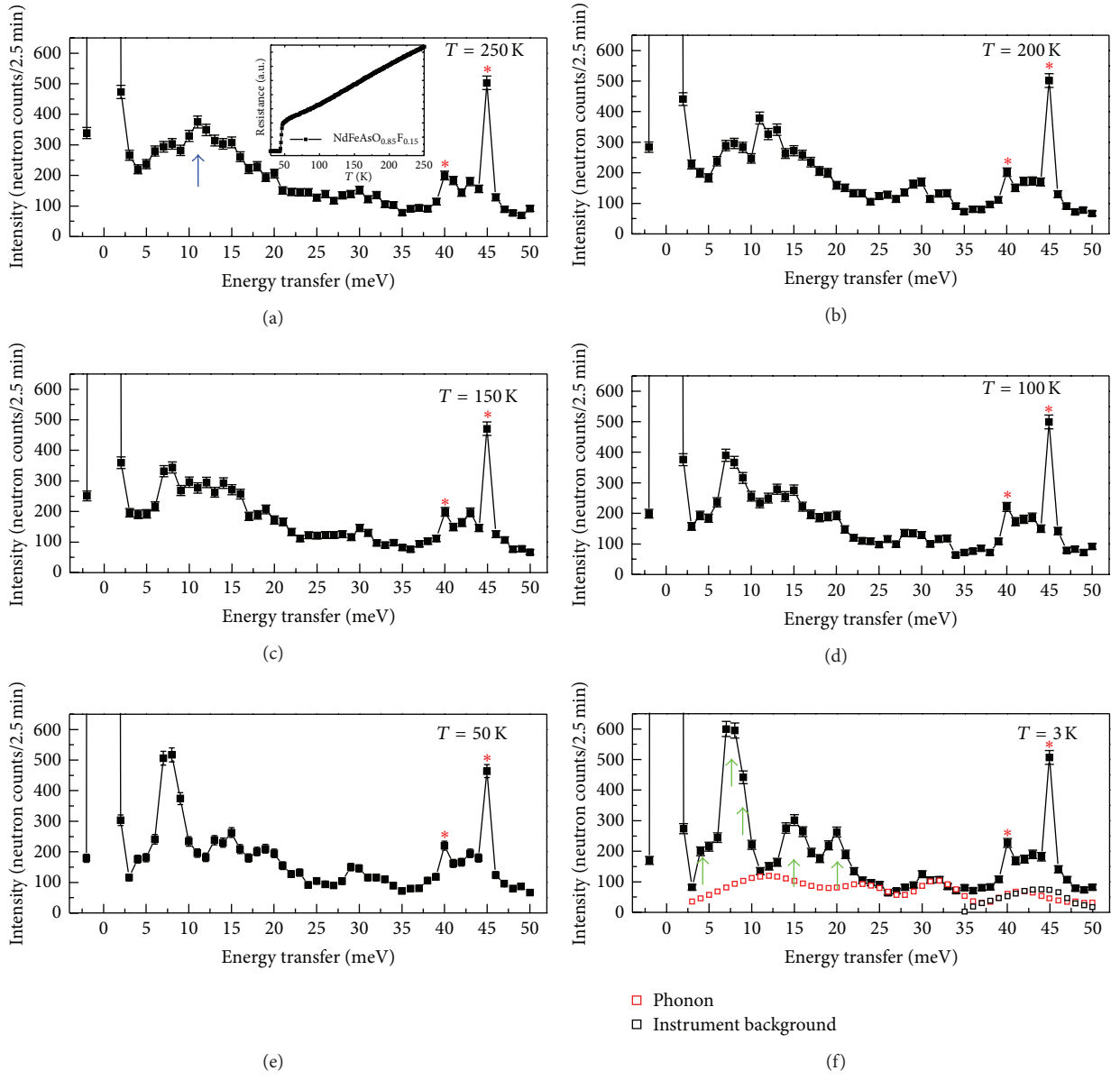

FIGURE 1: Inelastic neutron scattering spectra of $NdFeAsO_{0.85}F_{0.15}$ were measured with fixed $E_f = 14.7$ meV and $Q = 3.1$ Å. The energy scans were carried out at temperatures from 3 K to 250 K as marked on each figure. The solid lines are guides to the eye. The red stars marked the spurious peaks caused by the instrument setup. In the inset of Figure 1(a), the temperature dependence of resistance data of our samples is shown.

the weak crystal field approximation, which applies well to the R elements, the multiplets of different J's (total angular moment) are well separated in energy compared to the intra-multiplet splittings; therefore, the interactions between multiplets can be ignored. In such a case, the crystal field states can be considered based solely on the ground-state splitting [17].

According to Hund's rules, the ground state of Nd^{3+} ion, which contains three f-electrons, is $^4I_{9/2}$. The splitting of CF levels is directly related to the local lattice symmetry. $NdFeAsO_{0.85}F_{0.15}$ samples have a tetragonal crystal structure with $P4/nmm$ space group. The Nd atoms are located at the $2c$ crystallographic site therefore having C_{4v} point symmetry. This gives the crystal field Hamiltonian as follows:

$$H_{\mathrm{CEF}}(C_{4v}) = B_2^0 O_2^0 + B_4^0 O_4^0 + B_6^0 O_6^0 + B_4^4 O_4^4 + B_6^4 O_6^4, \quad (2)$$

where B_n^m are the CF parameters and O_n^m are Steven's operator equivalents. This CF symmetry splits the $^4I_{9/2}$ ground-state multiplet of the Nd^{3+} ion into five Kramers doublets.

However, suppose the CF peaks at $T = 3$ K in our $NdFeAsO_{0.85}F_{0.15}$ samples all came from the transitions between the five doublets as in the high temperature tetragonal phase of NdFeAsO [9]; then the number of ground-state excitation peaks should be at most four. According to

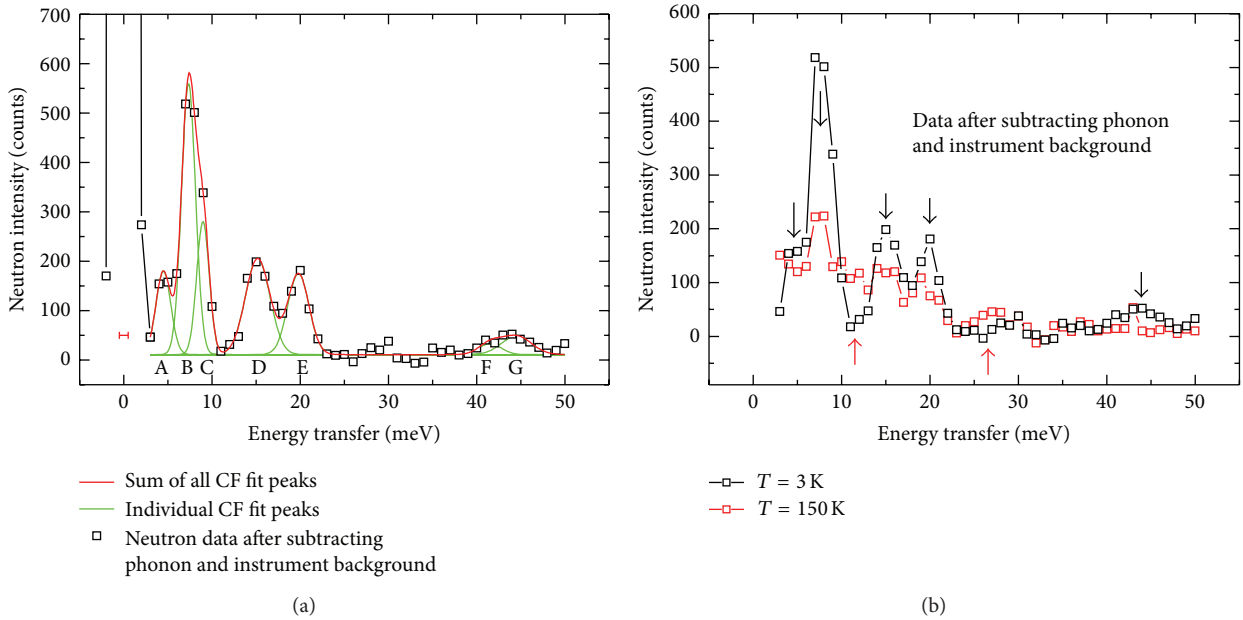

Figure 2: (a) Energy spectra of CF excitations in $NdFeAsO_{0.85}F_{0.15}$ at $T = 3$ K after subtracting the phonon and instrument background. The spectra were well fitted by seven Gaussian peaks. The instrumental energy resolution is 0.98 meV at elastic position (horizontal bar). (b) Comparison of the energy spectra of CF excitations between $T = 3$ K and $T = 150$ K after subtracting the phonon and instrument background. The black lines are guides to the eye.

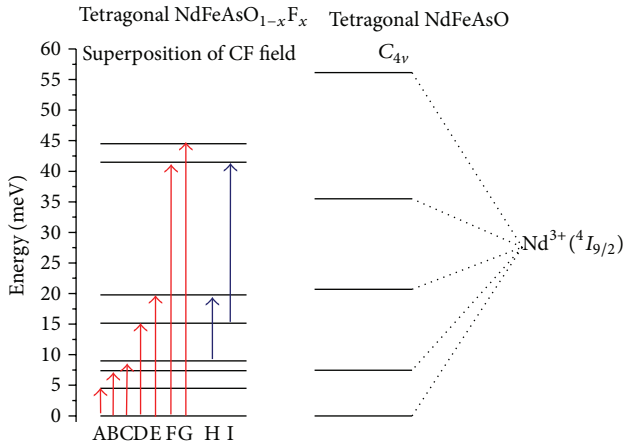

Figure 3: The Nd^{3+} CF energy level schemes for both NdFeAsO and $NdFeAsO_{0.85}F_{0.15}$ are shown. The values of energies of Nd^{3+} in $NdFeAsO_{0.85}F_{0.15}$ are sorted in increasing order: 0, 4.49, 7.34, 8.97, 15.17, 19.79, 41.50, and 44.51 meV. The energies of CF levels of NdFeAsO were obtained from another paper [9].

our data, the observed CF transitions for $NdFeAsO_{0.85}F_{0.15}$ outnumbered the transitions allowed for Nd^{3+} with C_{4v} point symmetry. Therefore the Hamiltonian in (2) is insufficient to describe the CF states in F-doped samples.

A reliable interpretation of the experimental data would be the occurrence of a superposition of crystal fields due to different local symmetries around the Nd^{3+} ions induced by the fluorine doping, similar to the case of oxygen defects in the R compounds $RBa_2Cu_3O_x$ [18] and $RCoO_x$ [19]. There are four nearest-neighboring oxygen ions around the Nd^{3+} ion; the ways of substitution of fluorine for oxygen could not all be the same. So different local charge environments and CF potentials around Nd^{3+} ions are expected. As in the analysis of $RCoO_x$ [19], in this situation because of the lowered point symmetry, additional terms are needed to enter the Hamiltonian in (2) which would produce more CF states as in our experimental data. Although it is difficult to give a parameterization in terms of the current complex CF Hamiltonian based on our data, the clear observation of seven ground-state CF transitions would provide strong evidence for the above analysis.

Besides $NdFeAsO_{0.85}F_{0.15}$, the additional CF states induced by F-doping were also observed in $PrFeAsO_{0.87}F_{0.13}$ [8]. However it is interesting to mention that, for another typical FeAs-1111 compound CeFeAs(O,F) [7], there is not much difference between the CF states in tetragonal CeFeAsO phase and $PrFeAsO_{0.86}F_{0.14}$ phase. The reason could be that the line widths of major CF transitions in the Ce compounds are of the order of 10 meV, which is significantly larger than that in Nd compounds (mainly below 3 meV). So the presumably small effect of fluorine doping could not be detected.

3. Concluding Remarks

Inelastic neutron scattering measurements were carried out on polycrystalline samples of $NdFeAsO_{0.85}F_{0.15}$ at different temperatures. Through the analysis of inelastic neutron spectra, up to seven ground-state CF excitations were identified. A crystal field energy level scheme for Nd^{3+} was proposed

which shows quite different features comparing with that in tetragonal NdFeAsO phase. This indicates the occurrence of superposition of crystal fields due to the inhomogeneous ligand charge environments and lowered local point symmetries around the Nd^{3+} upon fluorine doping.

Conflict of Interests

The authors declare that there is no conflict of interests regarding the publication of this paper.

Acknowledgments

The authors appreciate the useful discussions with R. Osborn, Songxue Chi, Ninghua Tong, Huining Dong, Tianlong Xia, and Yinguo Xiao. This work is supported by NSFC (no. 11204373), the Fundamental Research Funds for the Central Universities, and the Research Funds of Renmin University of China.

References

[1] D. R. Temprano, J. Mesot, S. Janssen et al., "Large isotope effect on the pseudogap in the high-temperature superconductor $HoBa_2Cu_4O_8$," *Physical Review Letters*, vol. 84, no. 9, pp. 1990–1993, 2000.

[2] Y. Kagan, K. A. Kikoin, and A. S. Mishchenko, "Interplay between heavy fermions and crystal-field excitation in Kondo lattices: Low-temperature thermodynamics and inelastic neutron scattering spectra of CeNiSn," *Physical Review B—Condensed Matter and Materials Physics*, vol. 55, no. 18, pp. 12348–12362, 1997.

[3] Y. Kamihara, T. Watanabe, M. Hirano, and H. Hosono, "Iron-based layered superconductor $La[O_{1-x}F_x]FeAs$ ($x = 0.05$–0.12) with $T_c = 26$ K," *Journal of the American Chemical Society*, vol. 130, no. 11, pp. 3296–3297, 2008.

[4] Z. A. Ren, J. Yang, W. Lu et al., "Superconductivity at 52 K in iron-based F-doped layered quaternary compound Pr[O1-xFx]FeAs," *Materials Research Innovations*, vol. 12, article 105, 2008.

[5] Z. A. Ren, J. Yang, W. Lu et al., "Superconductivity in the iron-based F-doped layered quaternary compound $Nd[O_{1-x}F_x]FeAs$," *EPL (Europhysics Letters)*, vol. 82, no. 5, Article ID 57002, 2008.

[6] Z. A. Ren, W. Lu, J. Yang et al., "Superconductivity at 55 K in iron-based F-doped layered quaternary compound $Sm[O_{1-x}F_x]$ FeAs," *Chinese Physics Letters*, vol. 25, no. 6, pp. 2215–2216, 2008.

[7] S. X. Chi, D. T. Adroja, T. Guidi et al., "Crystalline electric field as a probe for long-range antiferromagnetic order and superconducting state of $CeFeAsO_{1-x}F_x$," *Physical Review Letters*, vol. 101, no. 21, Article ID 217002, 2008.

[8] E. A. Goremychkin, R. Osborn, C. H. Wang et al., "Spatial inhomogeneity in $RFeAsO_{1-x}F_x$ (R = Pr, Nd) determined from rare-earth crystal-field excitations," *Physical Review B*, vol. 83, no. 21, Article ID 212505, 2011.

[9] Y. Xiao, M. Zbiri, R. A. Downie, J.-W. G. Bos, T. Brueckel, and T. Chatterji, "Inelastic neutron scattering study of crystal field excitations of Nd^{3+} in NdFeAsO," *Physical Review B*, vol. 88, Article ID 214419, 2013.

[10] S. A. Danilkin and M. Yethiraj, "TAIPAN: thermal triple-axis spectrometer," *Neutron News*, vol. 20, no. 4, pp. 37–39, 2009.

[11] R. Osborn, S. Rosenkranz, E. A. Goremychkin, and A. D. Christianson, "Inelastic neutron scattering studies of the spin and lattice dynamics in iron arsenide compounds," *Physica C*, vol. 469, no. 9–12, pp. 498–506, 2009.

[12] J. Noffsinger, F. Giustino, S. G. Louie, and M. L. Cohen, "Role of fluorine in the iron pnictides: phonon softening and effective hole doping," *Physical Review Letters*, vol. 102, no. 14, Article ID 147003, 2009.

[13] A. D. Christianson, M. D. Lumsden, O. Delaire et al., "Phonon density of states of $LaFeAsO_{1-x}F_x$," *Physical Review Letters*, vol. 101, no. 15, Article ID 157004, 2008.

[14] L. Soderholm, C.-K. Loong, and S. Kern, "Inelastic-neutron-scattering study of the Er^{3+} energy levels in $ErBa_2Cu_3O_7$," *Physical Review B*, vol. 45, Article ID 10062, 1992.

[15] E. A. Goremychkin and R. Osborn, "Crystal field excitations in YbT_2Si_2 (T = Fe, Co, Ni)," *Journal of Applied Physics*, vol. 87, no. 9, pp. 6818–6820, 2000.

[16] Y. Qiu, W. Bao, Q. Huang et al., "Crystal structure and antiferromagnetic order in $NdFeAsO_{1-x}F_x$ ($x = 0.0$ and 0.2) superconducting compounds from neutron diffraction measurements," *Physical Review Letters*, vol. 101, no. 25, Article ID 257002, 2008.

[17] L. Soderholm, C.-K. Loong, G. L. Goodman, and B. D. Dabrowski, "Crystal-field splittings and magnetic properties of Pr^{3+} and Nd^{3+} in $RBa_2Cu_3O_7$," *Physical Review B*, vol. 43, no. 10, pp. 7923–7935, 1991.

[18] J. Mesot, P. Allenspach, U. Staub, A. Furrer, and H. Mutka, "Neutron spectroscopic evidence for cluster formation and percolative superconductivity in $ErBa_2Cu_3O_x$," *Physical Review Letters*, vol. 70, no. 6, pp. 865–868, 1993.

[19] A. Furrer, A. Podlesnyak, M. Frontzek et al., "Crystal-field interaction and oxygen stoichiometry effects in strontium-doped rare-earth cobaltates," *Physical Review B*, vol. 90, no. 6, Article ID 064426, 2014.

Hindawi Publishing Corporation
Advances in Condensed Matter Physics
Volume 2015, Article ID 963768, 4 pages
http://dx.doi.org/10.1155/2015/963768

Research Article

The Insulator to Superconductor Transition in Ga-Doped Semiconductor Ge Single Crystal Induced by the Annealing Temperature

Y. B. Sun,[1,2] Z. F. Di,[1] T. Hu,[1] and X. M. Xie[1]

[1] *State Key Laboratory of Functional Materials for Informatics, Shanghai Institute of Microsystem and Information Technology, Chinese Academy of Sciences, Shanghai 200050, China*
[2] *University of Chinese Academy of Sciences, Beijing 100049, China*

Correspondence should be addressed to T. Hu; thu@mail.sim.ac.cn

Received 26 December 2014; Revised 8 March 2015; Accepted 19 March 2015

Academic Editor: Viorel Sandu

We have fabricated the heavily Ga-doped layer in Ge single crystal by the implantation and rapid thermal annealing method. The samples show a crossover from the insulating to the superconducting behavior as the annealing temperature increases. Transport measurements suggest that the superconductivity is from the heavily Ga-doped layer in Ge.

1. Introduction

Since the superconductivity was observed in metal in 1911, intensive efforts have been performed to find new superconductor such as high T_c cuprate [1] and pnictide [2]. The application of superconductor on the traditional industry now motivates scientists to find the superconductivity in semiconductor materials, since it can solve the problem of power consumption of integrated circuit and improve the efficiency of the device. As the superconductivity is induced in the diamond doped with boron [3] and the silicon doped with boron [4], the Ga-implanted germanium [5] with a total dose of 2×10^{16} cm^{-2} Ga was recently found to show superconductivity at the low temperature with the superconducting transition temperature lower than the germanium heavily doped with 4×10^{16} cm^{-2} Ga [6]. The origin of superconductivity in the heavily doped semiconductors, however, is an open question yet, even after the intensive study [6–8]. In this work, we fabricated the heavily Ga-doped Ge with a 30 nm SiO_2 cover layer by implanting Ga into the Ge single crystals and performed the rapid thermal annealing (RTA) on these samples. After performing the scanning electron microscope (SEM) and transport measurement, we find that the annealing temperature can induce an insulator to superconductor transition in Ga-doped Ge samples. Our study of superconductivity in the Ga-implanted Ge combines the superconductor and semiconductor which will contribute to application of superconductor on the traditional semiconductor industry.

2. Experimental Details

We chose the (1, 0, 0) oriented and P doped germanium as the substrate in this experiment. On the top of the germanium we grew a 30 nm SiO_2 cover layer through plasma-enhanced chemical vapor deposition (PECVD). After that, we implanted 4×10^{16} Ga cm^{-2} at an ion energy of 100 keV into it. Here, the SiO_2 capping layer can prevent the surface degradation [6] except the implanted region during implantation as shown in Figure 1.

We annealed the Ga-doped Ge samples by the rapid thermal annealing (RTA) for 60 s in flowing Ar atmosphere at various temperatures. The RTA was reported to play an important role in recrystallizing the amorphous implanted layer, which leads to the formation of the highly Ga-doped layer at the SiO_2/Ge interface [6, 8]. We therefore investigate the surface structure of the samples by the scanning electron microscope (SEM). The surface degradation does not occur

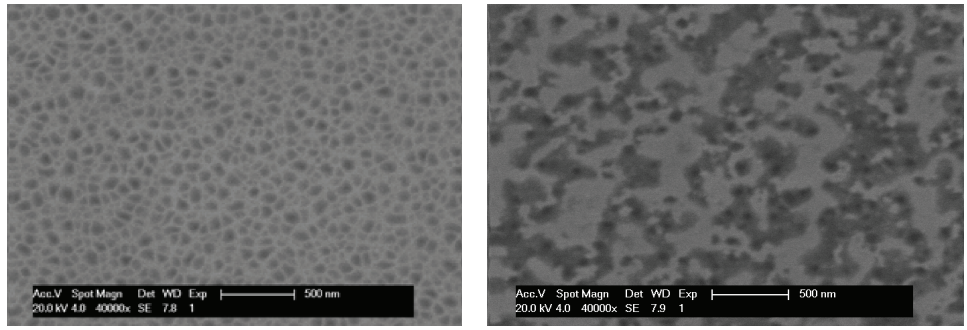

(a) (b)

FIGURE 1: Surface structure investigated with SEM in the (100) oriented Ge single crystal, which exposed at 4×10^{16} cm^{-2} Ga dose at an ion energy of 100 keV. (a) As-implanted sample. (b) Sample annealed at 800°C RTA in the flowing *Ar* atmosphere.

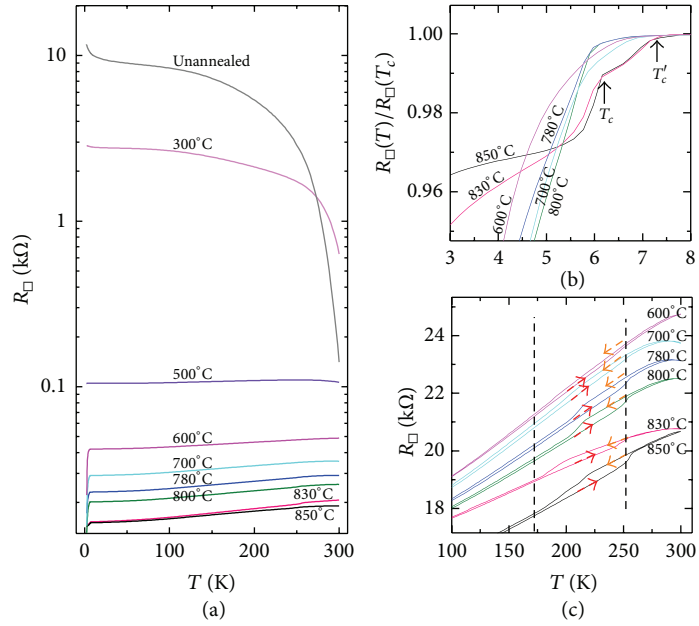

FIGURE 2: (a) T dependence of the sheet resistance $R_\square$ for samples with the different annealing temperatures. (b) The enlarged plot of (a) near the superconducting transition temperature T_c. (c) The thermal hysteresis curves for the samples annealed at temperature window (600°C–850°C). The arrows show the direction of the thermal cycle.

on the surface of the sample because of the protection of the SiO_2 capping as discussed before. But there are many discrete holes on the surface as a result of high dose implantation. For the as-implanted samples, the holes are discrete islands containing gallium; but for the samples annealed at 800°C, the gallium islands inside the holes percolate which can be regarded as superconducting grains of gallium percolating in the normal state germanium matrix.

To clarify the properties of the different annealed samples, we performed the electronic transport measurements on those annealed samples. We contacted the electrodes by the bonding lines and carried out the measurements in the usual four-terminal geometry at the temperature from 2.5 K to 300 K in a physical property measurement system (PPMS). The resistance was measured by ETO option whose excitation current is 100 μA. The temperature dependence of resistance in the as-implanted state and annealed at various temperatures under Ar flowing atmosphere is presented in Figure 2.

Figure 2(a) is the T dependence of the sheet resistance $R_\square$ for the unannealed and annealed samples. The $R_\square$s decreases as the annealing temperature increases. The logarithmic scale of $R_\square$ here shows how dramatic the electronic transport can be influenced by the annealing temperature. For different annealing temperature, it shows a transition from the insulating to superconducting behavior. Upon cooling, the as-implanted samples show an increasing resistance, which could reflect intrinsic semiconductor property of Ge, while upon increasing the annealing temperature, the sheet resistance decreases, which could be due to the change of the discrete Ga islands to percolating ones as discussed above.

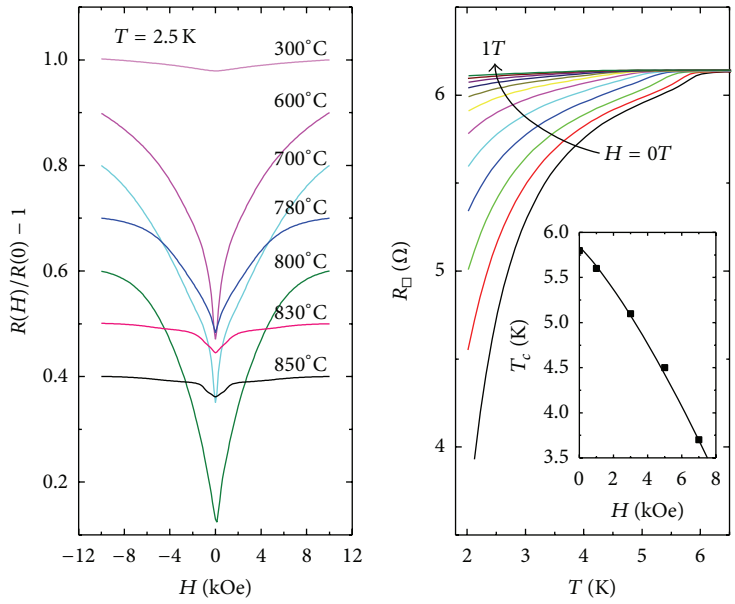

(a) (b)

FIGURE 3: (a) The H dependence of normalized magnetic resistance $(R(H)/R(0) - 1)$ measured at $T = 2.5$ K for the samples annealed at temperature ranging from 300°C to 850°C. (b) T dependence of the sheet resistance $R_{\square}$ at various magnetic fields H applied perpendicular to the surface for the samples annealed at 800°C. The inset shows the field-temperature $(H - T)$ phase diagram.

At the annealing temperatures ranging from 600°C to 850°C, the samples show a superconducting transition below 7 K as shown in Figure 2(b). There is a gradual drop of sheet resistance but zero resistance is not possible because of the discontinued superconducting path in the sample. When focusing on the low temperature transport carefully, we observed a detailed dependence of the superconducting properties on the annealing conditions. There is an optimal annealing temperature window (600°C–800°C). Out of that temperature window, the superconductivity is weak. There are two critical temperatures in the samples with annealing temperature at 830°C and 850°C.

It was shown in Figure 2(c) that the samples with superconducting behavior display a thermal hysteresis loop during the thermal cycle and the arrows mark the direction of those thermal cycles. The thermal hysteresis observed here shows the presence of the first order phase transition which could be attributed to the phase transition of the Ga grains from endothermic and exothermic process [9]. The gallium with exothermic process actually shows a similar superconducting transition temperature [10, 11] as the T_c in Figure 2(b). The superconducting gallium grains actually play an important role in the process. Based on [9], the β-Ga, γ-Ga, and δ-Ga show the similar hysteresis loop in the single-energy X-ray absorption measurements and the reason is their endothermic and exothermic process during thermal cycle. So we attribute the hysteresis loop to the gallium and relate the superconductivity to the hysteresis loop. Particularly the T_c of β-Ga is 6 K. It therefore clarifies the reason that the superconducting behavior is related to thermal hysteresis as observed in this experiment.

To obtain the further understanding of the character of superconducting state, we measured the magnetic field H dependence of the sheet resistance of the samples annealed from 300°C to 850°C. The normalized magnetoresistance $(R(H)/R(0) - 1)$ is plotted in Figure 3(a). (The data is shifted for clarity.) Here the H is perpendicular to the ab-plane of samples. As shown in Figure 3(a), the samples show the largest magnetoresistance variation at the annealing temperature window between 600°C and 800°C, which might suggest the strongest superconducting character there. We also performed the T dependence of sheet resistance $R_{\square}$ measurement for the sample annealed at 800°C with the applied magnetic fields H perpendicular to the ab-plane of the sample (Figure 3(b)). It is shown in Figure 3(b) that the superconducting transition is suppressed by the applied field H. We can define the critical temperature T_c as the 2% drop of normal state resistance for the sample measured at different H. The inset in Figure 3(b) is the $H - T$ phase diagram of the samples. The H_{c2} (0 K) at zero temperature was estimated as the 10% drop of H_{c2} at 2 K, which is approximately $0.5T$. Such a criterion is the same as the early work [6]. By using the standard theory, we can calculate the value of the Ginzburg-Landau coherence length ξ_{GL}. We deduce the $\xi_{GL} = 26$ nm via $\phi_0 = 2\pi H_{c2}\xi_{GL}^2$, where ϕ_0 is the magnetic flux quantum.

3. Summary

In summary, we have fabricated heavily Ga-doped Ge with a 30 nm SiO_2 cover layer. The ion implantation and subsequent RTA annealing were employed to form a Ga-doped layer at the SiO_2/Ge interface. The RTA annealing enables Ga to

redistribute in the sample and realize the superconducting circuits. Ga forms metallic precipitates in the Ge matrix. With increasing annealing temperature, the samples show a crossover from the insulator to the superconductor. The T_c is the same with the gallium's transition temperature and the hysteresis loop is related to gallium. So, the electronic transport measurements indicate that the Ga-doped layer plays a leading role in the superconductivity.

Conflict of Interests

The authors declare that there is no conflict of interests regarding the publication of this paper.

Acknowledgment

This work is supported by the "Strategic Priority Research Program (B)" of the Chinese Academy of Sciences Grant no. XDB04040300.

References

[1] J. G. Bednorz and K. A. Müller, "Possible high T_c superconductivity in the Ba-La-Cu-O system," *Zeitschrift für Physik B: Condensed Matter*, vol. 64, no. 2, pp. 189–193, 1986.

[2] Y. Kamihara, T. Watanabe, M. Hirano, and H. Hosono, "Iron-based layered superconductor La[$O_{1-x}F_x$]FeAs (x= 0.05-0.12) with T_c = 26 K," *Journal of the American Chemical Society*, vol. 130, no. 11, pp. 3296–3297, 2008.

[3] E. A. Ekimov, V. A. Sidorov, E. D. Bauer et al., "Superconductivity in diamond," *Nature*, vol. 428, no. 6982, pp. 542–545, 2004.

[4] E. Bustarret, C. Marcenat, P. Achatz et al., "Superconductivity in doped cubic silicon," *Nature*, vol. 444, no. 7118, pp. 465–468, 2006.

[5] T. Herrmannsdörfer, V. Heera, O. Ignatchik et al., "Superconducting state in a gallium-doped germanium layer at low temperatures," *Physical Review Letters*, vol. 102, no. 21, Article ID 217003, 2009.

[6] J. Fiedler, V. Heera, R. Skrotzki et al., "Superconducting Ga-overdoped Ge layers capped with SiO_2: structural and transport investigations," *Physical Review B*, vol. 85, no. 13, Article ID 134530, 2012.

[7] J. Fiedler, V. Heera, R. Skrotzki et al., "Superconducting films fabricated by high-fluence Ga implantation in Si," *Physical Review B*, vol. 83, no. 21, Article ID 214504, 2011.

[8] V. Heera, A. Mücklich, M. Posselt et al., "Heavily Ga-doped germanium layers produced by ion implantation and flash lamp annealing: structure and electrical activation," *Journal of Applied Physics*, vol. 107, no. 5, Article ID 053508, 2010.

[9] A. Di Cicco, "Phase transitions in confined gallium droplets," *Physical Review Letters*, vol. 81, no. 14, pp. 2942–2945, 1998.

[10] H. M. Jaeger, D. B. Haviland, A. M. Goldman, and B. G. Orr, "Threshold for superconductivity in ultrathin amorphous gallium films," *Physical Review B*, vol. 34, no. 7, pp. 4920–4923, 1986.

[11] H. Parr and J. Feder, "Superconductivity in beta-Phase Gallium," *Physical Review B*, vol. 7, no. 1, pp. 166–181, 1973.